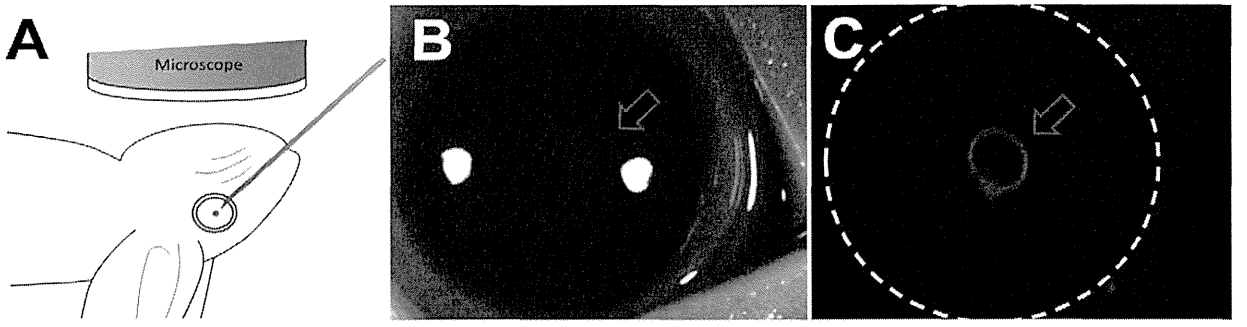

FIGURE 1. Measurement of migration of the fluorescein injected into rabbit stroma. (A) Schematic representation of an intracorneal injection of fluorescein solution. (B) A corneal photograph after stromal injection of the fluorescein. (C) A filtered photograph after stromal injection of stain. The *arrows* indicate the pooling of the stain.

observed for the first time the presence of intracorneal water movement from the center to the periphery in a swirling pattern in the horizontal plane, referred to as intracorneal swirling migration of water, and investigated its mechanisms in a normal cornea and an experimental model of corneal edema.

METHODS

Animals

Female Japanese albino rabbits weighing approximately 2.5 to 3.0 kg (Japan CLEA, Tokyo, Japan) were treated according to the Institutional Animal Care and Use Committee guidelines and the ARVO Statement for the Use of Laboratory Animals in Ophthalmic and Vision Research. The rabbits with clear corneas without ocular surface abnormalities were anesthetized using a 1 mL/kg intramuscular injection with an equal mixture of 500 mg of 5% ketamine (Ketalar hydrochloride; Sankyo Co., Ltd., Tokyo, Japan) and 2% xylazine (Selactar; Bayer Ltd., Tokyo, Japan) for all procedures. The rabbits were euthanized with an overdose of pentobarbital sodium.

Reagents

Ten percent fluorescein solution (Fluorescite; Alcon Japan Ltd., Tokyo, Japan), 10% benzalkonium chloride (BAC) solution; ouabain, a sodium-potassium pump inhibitor; and physiologic saline were purchased from Alcon Japan Ltd., Wako Pure Chemicals (Osaka, Japan), Sigma-Aldrich Corp. (St. Louis, MO, USA), and Otsuka Pharmaceutical (Tokyo, Japan), respectively. The 0.01% BAC solution was prepared by adding 10 μL 10% BAC solution to 10 mL physiologic saline. The ouabain solution (100 or 500 μM) and acetazolamide solution (1%) were dissolved in physiologic saline.

Intrastromal Injection of Fluorescein Solution Into Rabbit Corneas and Intracameral Injection of BAC and Ouabain Solution Into Rabbit Anterior Chambers

Sodium fluorescein is a polar molecule at physiologic pH and is reasonably soluble in the aqueous.[17] The 10% fluorescein solution (0.2 μL) was administered by intrastromal injection into the rabbit corneas using a syringe (Hamilton, Reno, NV, USA) with a 33-gauge needle (Fig. 1A). The injected fluorescein dye appeared as ring-shaped fluorescence (Figs. 1B, 1C), because no fluorescence was observed in the center of the injected area, and the stromal fluid diluted the dye and allowed fluorescence to occur. This is considered to be due to the concentration quenching of fluorescein[18,19] as a notable characteristic of fluorescein dye; a high concentration of fluorescein would have a greater reduction in fluorescent intensity compared with a low concentration of fluorescein due to self-quenching at a high concentration. In all experiments in which fluorescein was injected intrastromally, we easily distinguished fluorescein diffusion into the corneal stroma (Supplementary Fig. S1) from that in the anterior chamber by visual examination. In addition, the fluorescein diffusion in the anterior chamber from the stromal injection point was clearly rapid and had a different pattern (Supplementary Fig. S2) compared with fluorescein diffusion into corneal stroma. We eliminated the injected eyes with fluorescein diffusion in the anterior chamber from this study. Benzalkonium chloride (0.01% in physiologic saline) and ouabain (100 or 500 μM in physiologic saline) were injected intracamerally into the anterior chamber through the sclerocorneal limbus using a 30-gauge needle.

Observation of Transverse Water Migration in the Corneal Stroma

The rabbits were positioned on their side in order to observe one eye from above. To study horizontal water migration in the cornea, the movement of fluorescein solution injected into the corneal stroma was observed and recorded over time under a fluorescence stereomicroscope (SteREO Lumar V12; Carl Zeiss MicroImaging, Tokyo, Japan). At least three rabbits were tested in each experimental group. Fluorescence images of the cornea obtained after intrastromal injection of fluorescein solution were converted into binary images by setting a threshold for pixel intensity in Adobe Photoshop (Adobe Systems, Inc., San Jose, CA, USA), and the fluorescent area was measured using ImageJ software (version 1.47, http://imagej.nih.gov/ij/; provided in the public domain by the National Institutes of Health, Bethesda, MD, USA). The fluorescent areas were expressed as a percentage of the entire corneal area. The Mann-Whitney *U* test was performed to evaluate the statistical significance of the difference between groups. A value of $P < 0.05$ was considered significant. The time-lapse images, which were captured every 10 seconds for 20 minutes with 200-ms exposures, were converted to video format using microscopy software (AxioVision; Carl Zeiss MicroImaging).

Bullous Keratopathy Model

The rabbit model for bullous keratopathy was prepared by inducing toxicity of the corneal endothelial cells as described previously.[5] Briefly, 0.01% BAC was injected into the anterior chamber, which induced total corneal edema. A few weeks later during recovery, very mild peripheral corneal edema served as the model.

Investigative Ophthalmology & Visual Science

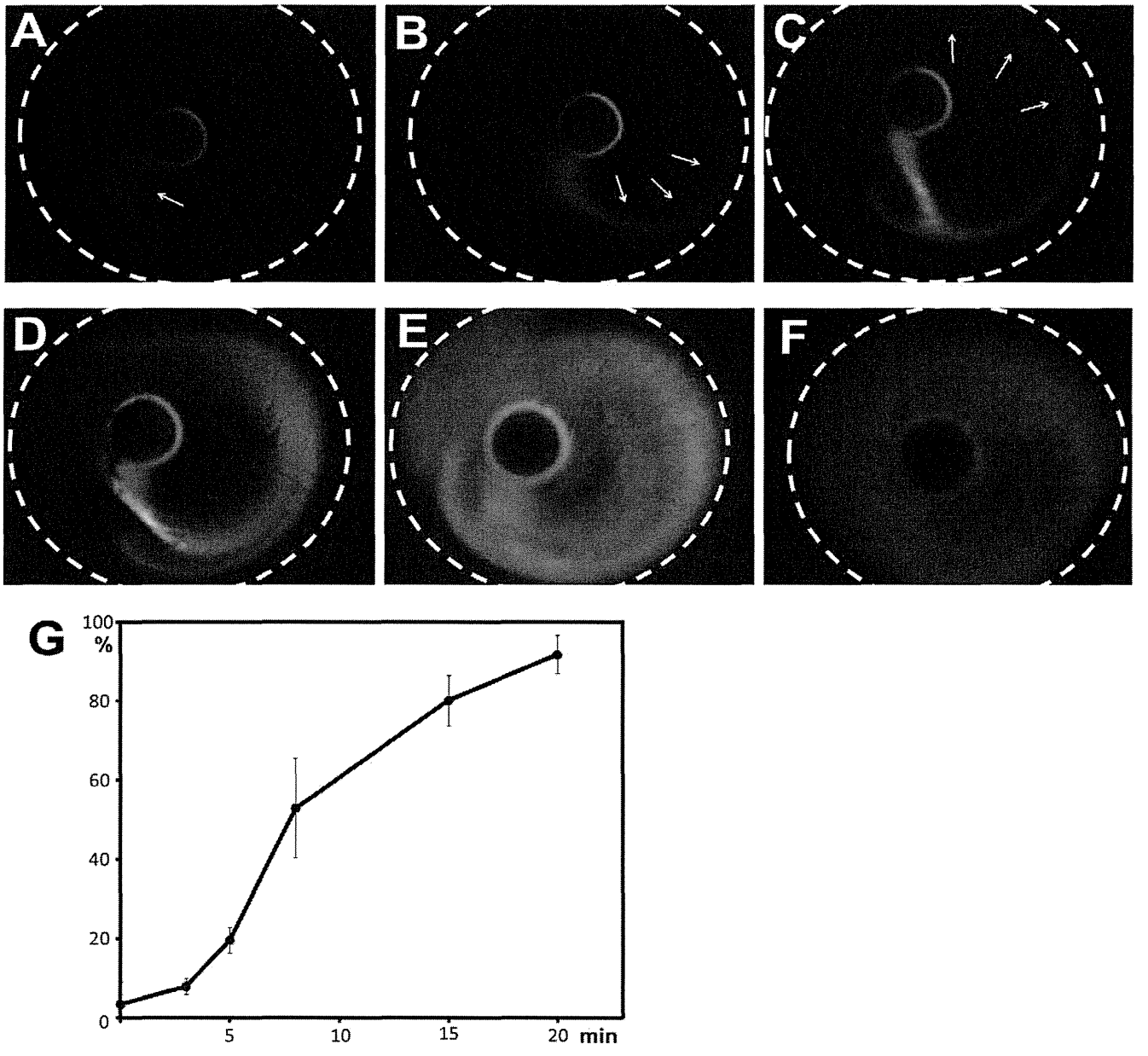

FIGURE 2. Intracorneal swirling flow of water in a normal cornea after fluorescein injection in the central area. (**A**) A photograph obtained 3 minutes after injection. The movement of the stain (*arrow*) begins in a linear fashion from the central pooling of the stain to the periphery. (**B**) A photograph obtained 4 minutes after injection. The fluorescein (*arrows*) reaches the most peripheral cornea. (**C**) A photograph obtained 5 minutes after injection. The movement (*arrows*) of the fluorescein swirling in an arc along the periphery. (**D**) A photograph obtained 8 minutes after injection. The movement of the fluorescein has expanded. (**E**) A photograph obtained 15 minutes and (**F**) 20 minutes after injection. The fluorescein covers the entire cornea. (**G**) The fluorescent area over time as a percentage of the entire cornea. The *y*-axis shows the percentages of the fluorescent area in relation to the entire cornea. The *x*-axis shows the time after injection (minutes). The movement of the water indicates the presence of horizontal water flow in the entire normal cornea, namely, the intracorneal swirling flow of water. The *error bars* indicate the standard error of the mean.

RESULTS

Corneal Water Migration in the Horizontal Plane in Normal Corneas

Using a fluorescence microscopic camera, we observed pooling of the fluorescein solution in the central cornea (Figs. 1B, 1C) after the stromal injection. The injected dye appeared as ring-shaped fluorescence due to the concentration quenching of fluorescein.[18,19] In normal corneas, the water began to flow from the point of central pooling to the corneal periphery in a linear fashion (Fig. 2A) 3 minutes after the injection. Upon reaching the peripheral cornea (Fig. 2B) 4 minutes after the injection, the water swirled in an arc along the most peripheral area (Fig. 2C) 5 minutes after the injection, and the range of the fluorescence flow (Fig. 2D) expanded 8 minutes after the injection and ultimately covered the entire cornea (Figs. 2E, 2F) 15 and 20 minutes, respectively, after the injection. These results indicated the presence of horizontal water migration in the entire normal cornea. Although we observed slow centrifugal diffusion of the fluorescein from the point of injection in all directions to the peripheral cornea, we primarily observed a rapid unidirectional spiral pattern of

fluorescein originating from the point of injection. The spiral pattern was driven by in vivo intracorneal water migration. The values of IOP measured by a tonometer (Icare Finland Oy, Vantaa, Finland) before the experiment (average ± SEM, 7.8 ± 0.5 mm Hg; $n = 5$) did not differ significantly from those measured after the experiment (8.5 ± 0.8 mm Hg). The measurements of the fluorescent area and estimations of their extent over time as a percentage of the entire corneal area were 3.4% ± 0.2%, 7.8% ± 1.1%, 19.6% ± 3.2%, 52.9% ± 12.6%, 80.1% ± 6.3%, and 91.8% ± 4.8% (average ± SEM; $n = 5$) at 0, 3, 5, 8, 15, and 20 minutes, respectively. Analysis of the expansion of the flow of water (Fig. 2G) indicated that the fluorescent-positive area gradually increased and encompassed the entire cornea throughout the time of observation. Supplementary Video S1 is a time-lapse video of the normal cornea after intrastromal injection of the fluorescein solution. The video shows the details of the dynamic appearance of the swirling flow of water.

To investigate the relation between the point at which the fluorescein solution was injected into the cornea and the patterns of the swirling water, we observed the patterns starting from the corneal periphery. After the fluorescein solution was injected into the peripheral cornea (Fig. 3A), the swirling flow of water appeared from that point in an arc (Fig. 3B), moved toward the center after one rotation (Figs. 3C–E), and gradually spread (Fig. 3F). There was no direct linear movement toward the center from the point of injection. With the injection into the peripheral cornea and that in the center, the horizontal swirling water eventually covered the entire cornea. After the initial linear flow reached the most peripheral area, the fluorescence intensity in the limbus increased, indicating partial movement of the water from the cornea to outside the cornea (i.e., the sclera).

When we injected the fluorescein into the sclera near the corneal limbus (Fig. 4A), no fluorescein signals in the cornea were recorded throughout the time course, indicating no horizontal water migration into the cornea from the periphery (Figs. 4B, 4C).

The animals were euthanized and fluorescein was injected into the corneal center 1 hour later when blood flow is interrupted and body temperature decreases. A few hours post mortem, the horizontal intracorneal swirling flow of water was still present as in a living normal eye (Figs. 5A, 5B), indicating that the swirling flow of water in the cornea does not result from blood flow in the peripheral limbus.

Corneal Endothelial Function Controls the Intracorneal Swirling Flow of Water

Over time, the linear flow of water to the peripheral cornea and the swirling flow of water to the entire cornea identified in a normal cornea were not seen in this model of bullous keratopathy (Fig. 6A). The fluorescein spread diffusely and was not immersed in the peripheral cornea. Active intracorneal swirling was not seen and only spread slowly in the bullous model (Figs. 6B–E). The values of IOP in eyes with bullous cornea before the experiment (average ± SEM, 9.2 ± 1.3 mm Hg; $n = 3$) did not differ significantly compared with those after the experiment (8.4 ± 0.5 mm Hg). The percentages of the fluorescent area in relation to the entire cornea were 7.4% ± 1.6%, 9.6% ± 2.0%, 11.3% ± 2.0%, 14.2% ± 2.0%, 18.1% ± 2.0%, and 22.1% ± 0.7% (average ± SEM; $n = 3$) at 0, 3, 5, 8, 15, and 20 minutes, respectively. Analysis of the amount of fluorescein in the bullous corneas (Fig. 6F) indicated that there were significantly ($P < 0.05$) fewer fluorescent areas in the bullous cornea compared with normal corneas. Supplementary Video S2 is a time-lapse video of a bullous cornea in which there is no intracorneal swirling migration and only diffusion. In this experiment in the bullous model, no horizontal water migration was seen, suggesting that the source of the horizontal water migration in the cornea may be associated with corneal endothelial function.

To determine which endothelial cellular function affected the horizontal water migration in the cornea, ouabain was infused to suppress the corneal endothelial pump function. The endothelial cellular pump function and the horizontal water migration were suppressed when 1000 μM of ouabain was injected into the anterior chamber. After injection, there was no active intracorneal swirling migration but only slow diffusion (Figs. 7A–D) as in the corneas with bullous keratopathy, indicating that the swirling flow of water is controlled by the corneal endothelial pump function. To investigate this in more detail, we performed an experiment using a low concentration of ouabain (100 μM) and compared the intracorneal swirling flow of water with that in a normal cornea (Figs. 7E–H). Analysis of the extent of the fluorescein showed that the percentages of the fluorescent area in relation to the entire cornea after treatment with 1000 μM of ouabain were 3.8% ± 0.5%, 7.6% ± 0.7%, 12.7% ± 0.6%, 11.4% ± 0.9%, 25.3% ± 5.6%, and 34.3% ± 8.2% (average ± SEM; $n = 4$) and after treatment with 100 μM of ouabain the percentages were 3.2% ± 0.5%, 9.6% ± 2.6%, 11.3% ± 2.4%, 23.0% ± 4.4%, 57.0% ± 10.0%, and 82.0% ± 5.4% (average ± SEM; $n = 4$) at 0, 3, 5, 8, 15, and 20 minutes, respectively (Fig. 7I). The speed with which the stain moved in eyes treated with 1000 μM of ouabain was suppressed significantly compared with normal eyes. With the lower concentration of ouabain, the area of diffusion increased significantly compared with the higher concentration. These results indicated that the driving force of the intracorneal swirling flow of water is dependent on the corneal endothelial cellular pump function.

When we then examined the relation between the intracorneal horizontal flow of water and partial peripheral corneal edema that remained during the recovery period after induction of corneal edema, the edema was confided to the upper periphery (Fig. 8A). The figure also shows horizontal water movement in a normal cornea, that is, in the area opposite to that with the peripheral edema, from the center to the periphery. Figure 8B also shows linear flow to the periphery and the swirling flow of water that gradually spread to the entire cornea over time as well as a normal pattern. However, no water flow was seen in areas with peripheral edema (Figs. 8C, 8D). Analysis of the amount of stain moving around the cornea showed that the percentages of the fluorescent area in relation to the entire cornea were 2.9% ± 0.6%, 7.7% ± 2.2%, 11.6% ± 1.8%, 22.1% ± 5.8%, 41.7% ± 11.2%, and 48.7% ± 6.9% (average ± SEM; $n = 3$) at 0, 3, 5, 8, 15, and 20 minutes, respectively; Fig. 8E). The fluorescent-positive area in the cornea with peripheral edema significantly decreased compared with that in normal cornea in the late phase of the observation (15 or 20 minutes).

Discussion

Although exacerbation and improvement of the corneal edema in the horizontal plane can be observed in clinical samples,[16] the reason for the preferential water retention in the peripheral cornea is unknown and has never been investigated. One attractive hypothesis is the presence of water migration from the center to the periphery in the horizontal corneal plane. The current experiments using fluorescein dye as a tracer showed for the first time the horizontal migration of water in normal corneas. The water movement was characterized by a swirling motion in the stroma and the fluorescein solution ultimately spread and encompassed the entire cornea.

Investigative Ophthalmology & Visual Science

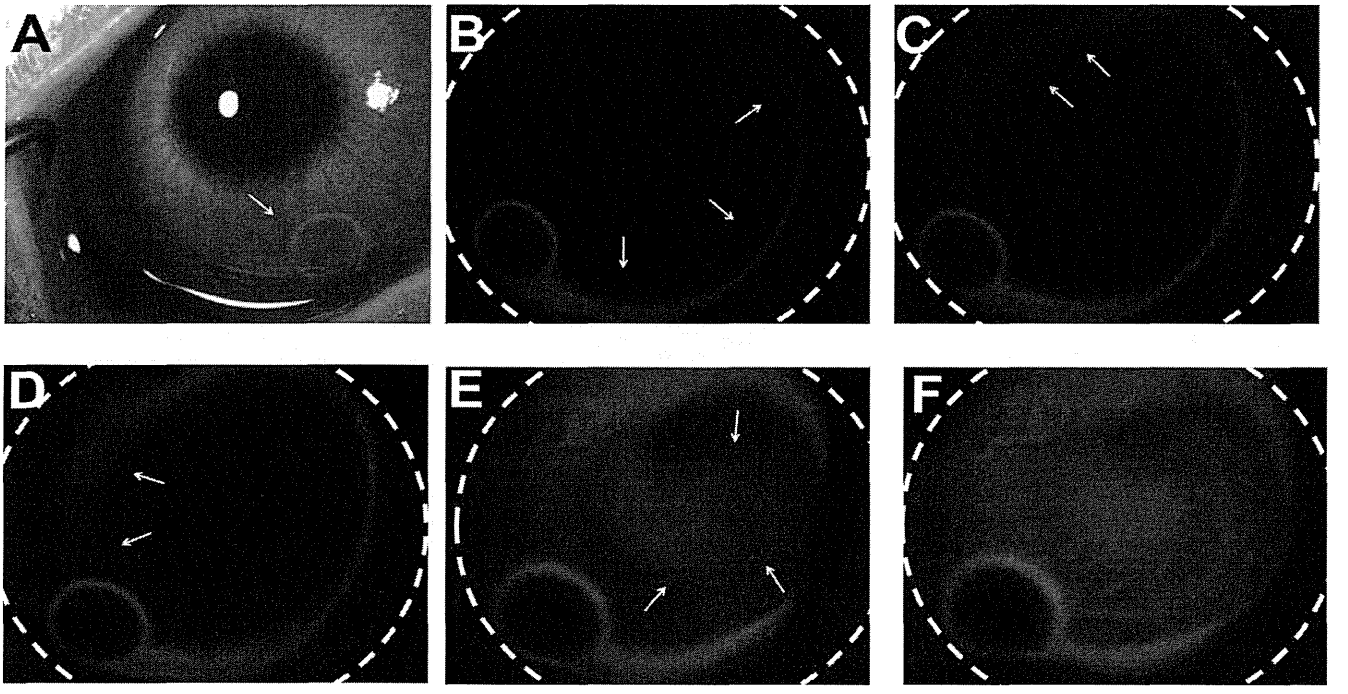

FIGURE 3. Intracorneal swirling flow of water after a fluorescein injection into the peripheral cornea. (**A**) A photograph obtained after fluorescein injection into the peripheral cornea. The *arrow* indicates the pooling point. (**B**) A photograph obtained 3 minutes and (**C**), 4 minutes after injection. The intracorneal swirling flow of water (*arrows*) begins to move from the injection point in the periphery along an arc. (**D**) A photograph obtained 5 minutes after injection. The arrows indicate the swirling flow of water. The swirling motion continues toward the center after one rotation. (**E**) A photograph obtained 8 minutes after injection. The *arrows* indicate the swirling flow of water. (**F**) A photograph obtained 15 minutes after injection. The swirling flow of water has expanded to the entire cornea.

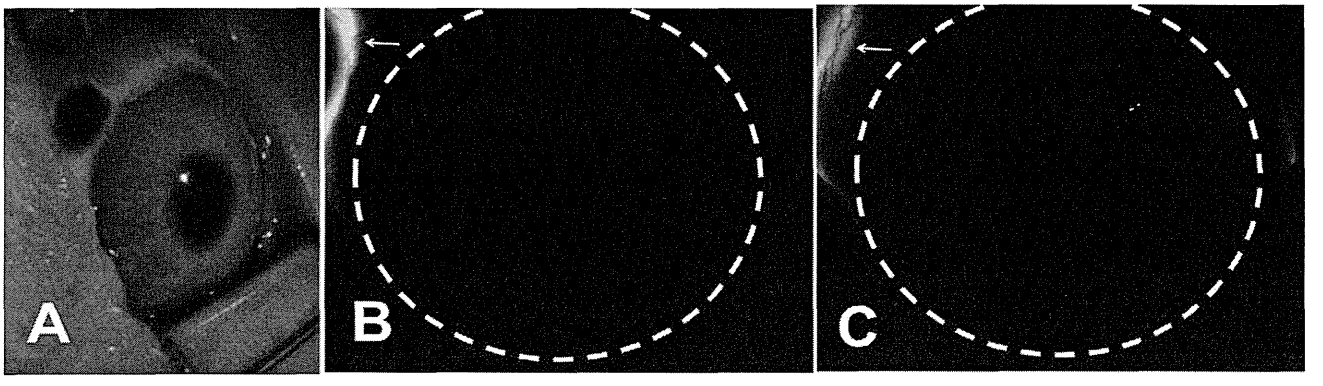

FIGURE 4. The intracorneal swirling flow of water is not induced by a fluorescein injection into the sclera near the corneal limbus. (**A**) The fluorescein solution is injected into sclera the near the corneal limbus. (**B**) A photograph obtained 5 minutes after injection and (**C**) 20 minutes after injection. No water stream from the sclera to the cornea is detected.

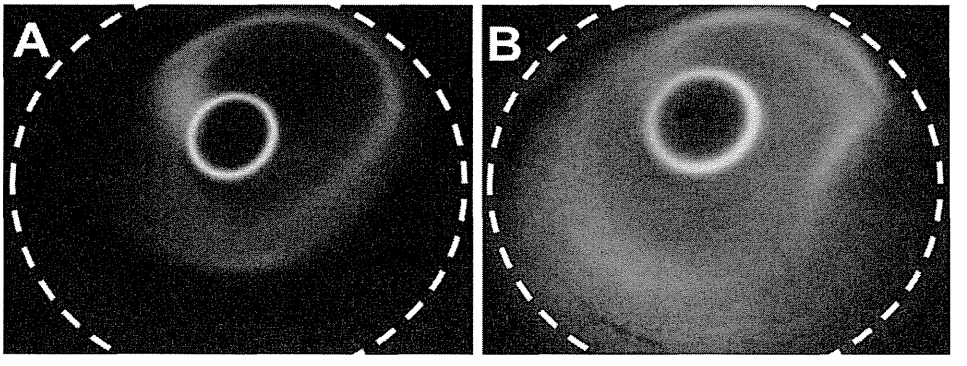

FIGURE 5. Intracorneal swirling flow of water after fluorescein injection in a postmortem cornea. The intracorneal swirling flow continues after death. (**A**) A photograph obtained 5 minutes and (**B**), 15 minutes after the injection.

Investigative Ophthalmology & Visual Science

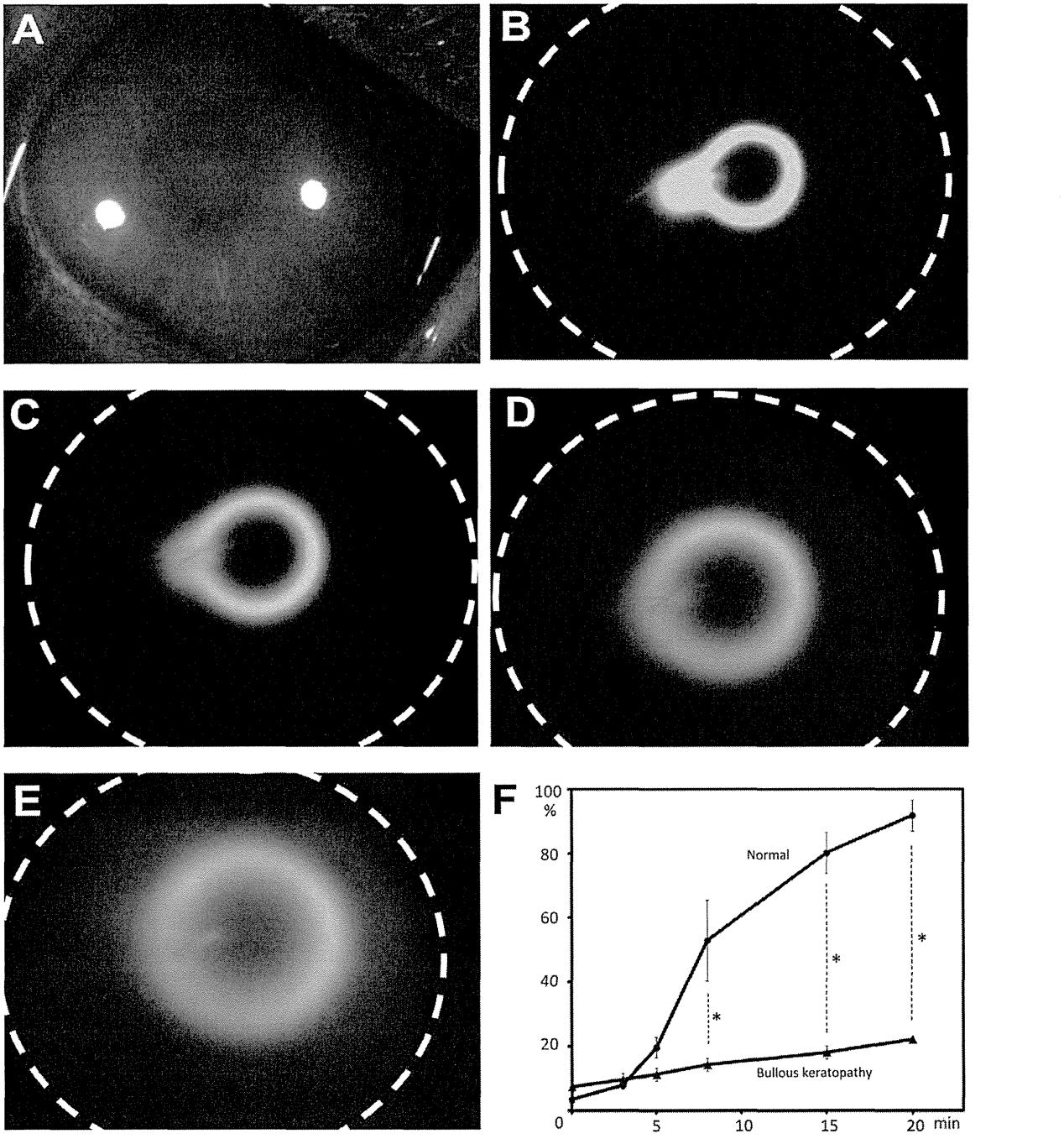

FIGURE 6. Intracorneal swirling flow of water after fluorescein injection into the cornea in the bullous keratopathy model. (**A**) A photograph obtained 7 days after the intracameral BAC injection in the bullous keratopathy model. (**B**) A photograph obtained 3 minutes, (**C**) 8 minutes, (**D**) 15 minutes, and (**E**) 20 minutes after injection. (**F**) Analysis of the fluorescent area over time as a percentage of the entire corneal area. $^*P < 0.05$. The intracorneal swirling flow of water seen in normal corneas is not seen over time. The stain only spreads diffusely and has not reached immersion in the corneal periphery. The *error bars* indicate the standard error of the mean.

In contrast, when the corneal endothelia were injured by intracameral injection of a preservative to create corneal edema, no swirling water migration was seen, suggesting that the integrity of the corneal endothelial function is essential for this water movement. The swirling migration of the water also stopped with injection of the sodium-potassium pump inhibitor, indicating the need for this enzyme for physiologic water migration in the cornea. When corneal endothelial function recovered, the swirling migration resumed while focal edema remained at the periphery, and no water migration occurred in the edematous area. These results suggested that water retention in the peripheral cornea may be related to the intracorneal swirling flow of water. The intracorneal water migration weakened with decreased corneal endothelial function and may result in partial peripheral corneal edema progressing to total corneal edema (Fig. 9).

Although we suggested that the driving force of intracorneal swirling migration of water is the endothelial cellular pump function, there are other possibilities. First may be the centrifugal force from the corneal center to the periphery.

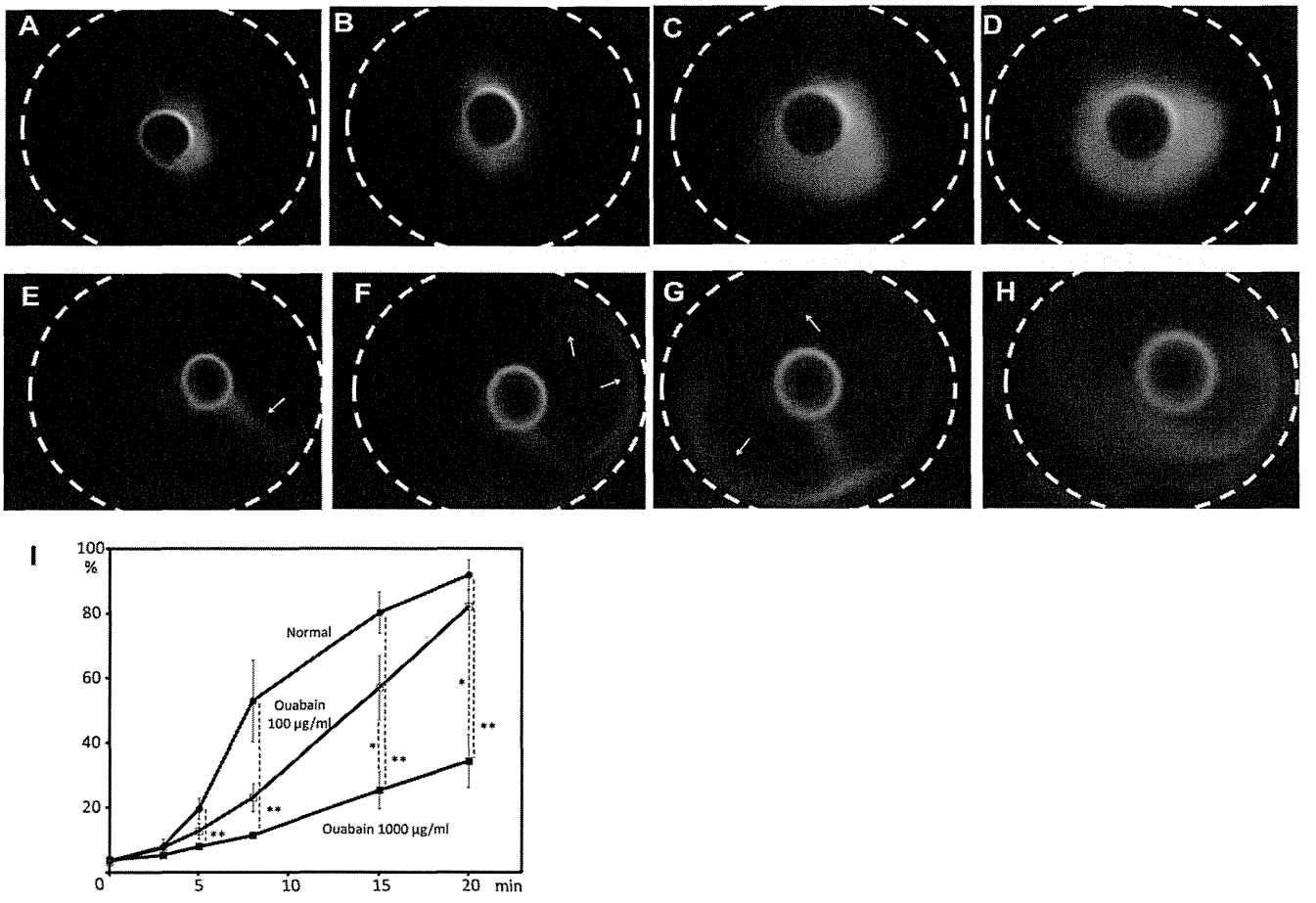

FIGURE 7. (A–D) Intracorneal swirling flow of water after fluorescein injection into the cornea after a 1000-µM intracameral injection of ouabain. (A) A photograph obtained 3 minutes, (B) 8 minutes, (C) 15 minutes, and (D) 20 minutes after the injection of stain. No active intracorneal swirling flow of water is seen over time. (E–H) The intracorneal swirling flow of water after fluorescein injection into the cornea of a 100-µM intracameral injection of ouabain. (E) A photograph obtained 3 minutes, (F) 8 minutes, (G) 15 minutes, and (H) 20 minutes after stain injection. The *arrows* indicate the flow of water. A weak intracorneal swirling flow of water is seen compared with that in normal corneas. (I) Analysis of the spread of the fluorescent solution. The speed of immersion of the fluorescein in eyes treated with a 1000-µM intracameral injection of ouabain is suppressed significantly compared with normal eyes. With the 100-µM concentration of ouabain, the diffusion increases significantly compared to the 1000-µM concentration. $^{*}P < 0.05$. $^{**}P < 0.01$. The *error bars* indicate the standard error of the mean.

However, when the fluorescein solution was injected into the peripheral cornea, the swirling flow of water generated from the injection in the periphery moved toward the center in an arc-shaped rotation contrary to the centrifugal force from the center to the periphery. Further investigations of the developmental mechanism of intracorneal swirling migration of water are needed. A second possibility may be the corneal structure. Water transfer from the center to the corneal periphery may occur because of structural differences between the two areas. Water absorbency varies depending on the nature of the proteoglycan and collagen fiber organization, which may affect water transfer in the cornea. The concentration of acidic glycosaminoglycans such as keratan sulfate and chondroitin is highest in the central cornea.[20] Further, the force behind the intracorneal swirling migration of water may result directly from a functional difference, such as the electrophysiologic activity between the periphery and the center. Further research is needed to clarify the difference between the center and the periphery.

Although the developmental mechanism of corneal edema and water migration in the cornea has been explained in terms of water movement in a vertical cross section of the cornea,[1,7] we showed the presence of horizontal water migration. A stain injected into the central cornea first moved linearly from the central cornea to the periphery in the flow of water. After reaching the periphery, the stain moved by circulating along the corneal edge and along the arc and diffused into the cornea as an intracorneal horizontal swirling migration of water. When the fluorescein solution was injected in the periphery, the swirling flow of water began along an arc and diffused into the entire cornea. These results may be evidence of an efficient dynamic water circulatory system that covers a large area and contributes to water retention, nutrient supply, and waste removal in the avascular corneal tissue. Transverse movement of a macro in the cornea would increase the efficiency of the metabolism of the entire cornea, which may be biologically reasonable. In this study, we indirectly observed the water migration using the fluorescein agent. However, there is no direct evidence whether the fluorescein agent can represent the natural water movement itself in the cornea. The local gradient in inhibition pressure created artificially in these experiments may not necessarily represent the natural physiologic process. This is the limitation of our investigation. Although the intracorneal swirling migration of water represents water flow in the corneal stroma, it remains to be determined which part of the corneal stroma this flow moves through. The specific composition of the corneal fibers

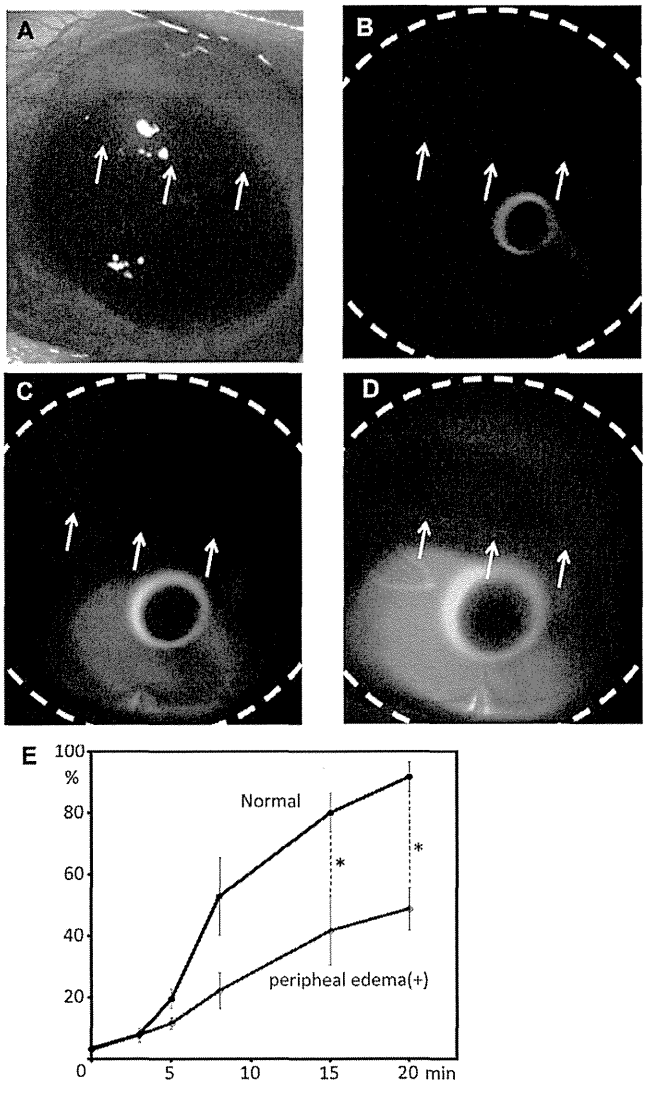

FIGURE 8. (A) A photograph of a cornea with peripheral edema confined to the upper area. (B) A photograph obtained 5 minutes, (C) 8 minutes, and (D) 20 minutes after the fluorescein injection. The *arrows* indicate peripheral edema. (A) Although the intracorneal swirling flow of water began and (C, D) spread gradually to the entire normal cornea on the side opposite the peripheral edema, no water flow is seen in areas with peripheral edema. (E) Analysis of the movement of the stain. The speed of the movement of the stain in the corneas with peripheral edema is significant compared with normal eyes 15 or 20 minutes after injection. $^*P < 0.05$. The *error bars* indicate the standard error of the mean.

coursing through the corneal stroma has been investigated.[21] Further investigations are needed to clarify these issues.

Corneal edema is one of the most representative human corneal diseases characterized by water pooling in the cornea. Since our results suggested that intracorneal swirling migration of water as a physiologic phenomenon may be related to development of corneal edema, the variations in this horizontal water migration in the early progression stage or recovery process of corneal edema remain to be elucidated. Further investigations that continuously monitor the intracorneal swirling migration of water in different degrees of corneal edema may clarify the developmental mechanism of corneal edema.

In summary, we report for the first time the presence of horizontal intracorneal swirling flow of water in the cornea.

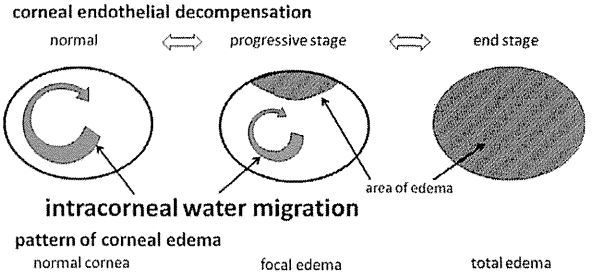

FIGURE 9. Schematic representation of the relation between the intracorneal swirling flow of water and corneal endothelial decompensation. The intracorneal water migration weakens with decreased corneal endothelial function and may result in partial peripheral corneal edema progressing to total corneal edema.

The water migration was generated by the sodium-potassium pump function in the corneal endothelial cells. This novel phenomenon may be the key to new interpretations of several pathological findings and/or treatments for corneal diseases in the future.

Acknowledgments

The authors alone are responsible for the content and writing of the paper.

Disclosure: **T. Inoue**, None; **T. Kobayashi**, None; **S. Nakao**, None; **Y. Hara**, None; **T. Suzuki**, None; **Y. Hayashi**, None; **X. Zheng**, None; **A. Shiraishi**, None; **Y. Ohashi**, None

References

1. Klyce SD. Corneal physiology, In: *The Cornea*. Philadelphia: Lippincott Williams & Wilkins; 2005.
2. Beebe DC. Maintaining transparency: a review of the developmental physiology and pathophysiology of two avascular tissues. *Semin Cell Dev Biol*. 2008;19:125-133.
3. Goldman JN, Benedek GB. The relationship between morphology and transparency in the nonswelling corneal stroma of the shark. *Invest Ophthalmol*. 1967;6:574-600.
4. Dohlman CH, Hedbys BO, Mishima S. The swelling pressure of the corneal stroma. *Invest Ophthalmol Vis Sci*. 1962;1:158-162.
5. Maurice D, Perlman M. Permanent destruction of the corneal endothelium in rabbits. *Invest Ophthalmol Vis Sci*. 1977;16:646-649.
6. Maurice DM. The permeability to sodium ions of the living rabbit's cornea. *J Physiol*. 1951;112:367-391.
7. Klyce SD, Russell SR. Numerical solution of coupled transport equations applied to corneal hydration dynamics. *J Physiol*. 1979;292:107-134.
8. Fatt I, Goldstick TK. Dynamics of water transport in swelling membranes. *J Colloid Sci*. 1965;20:962-989.
9. Hedbys BO, Dohlman CH. A new method for the determination of the swelling pressure of the corneal stroma in vitro. *Exp Eye Res*. 1963;2:122-129.
10. Mishima S, Hedbys BO. The permeability of the corneal epithelium and endothelium to water. *Exp Eye Res*. 1967;6:10-32.
11. Harris JE, Nordquist LT. The hydration of the cornea. I. The transport of water from the cornea. *Am J Ophthalmol*. 1955;40:100-110.
12. Hodson S, Miller F. The bicarbonate ion pump in the endothelium which regulates the hydration of rabbit cornea. *J Physiol*. 1976;263:563-577.

13. Manchester PT Jr. Hydration of the cornea. *Trans Am Ophthalmol Soc.* 1970;68:425-461.
14. Ytteborg J, Dohlman CH. Corneal edema and intraocular pressure. II. Clinical results. *Arch Ophthalmol.* 1965;74:477-484.
15. Maurice DM. The location of the fluid pump in the cornea. *J Physiol.* 1972;221:43-54.
16. Gothard TW, Hardten DR, Lane SS, et al. Clinical findings in Brown-McLean syndrome. *Am J Ophthalmol.* 1993;115:729-737.
17. Wilson G, Ren H, Laurent J. Corneal epithelial fluorescein staining. *J Am Optom Assoc.* 1995;66:435-441.
18. Nichols JJ, King-Smith PE, Hinel EA, et al. The use of fluorescent quenching in studying the contribution of evaporation to tear thinning. *Invest Ophthalmol Vis Sci.* 2012;53:5426-5432.
19. Chen RF, Knutson JR. Mechanism of fluorescence concentration quenching of carboxyfluorescein in liposomes: energy transfer to nonfluorescent dimers. *Anal Biochem.* 1988;172:61-77.
20. Morishige N, Yamada N, Zhang X, et al. Abnormalities of stromal structure in the bullous keratopathy cornea identified by second harmonic generation imaging microscopy. *Invest Ophthalmol Vis Sci.* 2012;53:4998-5003.
21. Borcherding MS, Blacik LJ, Sittig RA, et al. Proteoglycans and collagen fibre organization in human corneoscleral tissue. *Exp Eye Res.* 1975;21:59-70.

カラーコンタクトレンズ着色顔料厚と角膜上皮障害との関係

江口 洋[1], 宮本龍郎[1], Enkhmaa Tserennadmid[1], 蓑手孝宗[1], 谷 彰浩[1], 安部翔子[1], 堀田芙美香[1], 三田村佳典[1], 檜野 栞[2], 松永 透[2], 佐藤隆郎[2]
徳島大学大学院ヘルスバイオサイエンス研究部眼科学分野[1], 株式会社シード[2]

Relationship between Thickness of the Colored Layer on Cosmetic Tinted Contact Lenses and Corneal Epithelial Disorders

Hiroshi Eguchi[1], Tatsuro Miyamoto[1], Enkhmaa Tserennadmid[1], Takamune Minote[1], Akihiro Tani[1], Shoko Abe[1], Fumika Hotta[1], Yoshinori Mitamura[1], Shiori Hino[2], Toru Matsunaga[2] and Takao Sato[2]
Department of Ophthalmology, Institute of Health Biosciences, The University of Tokushima Graduate School[1], SEED Co., Ltd.[2]

カラーコンタクトレンズ（**cosmetic tinted contact lens**：カラー CL）の顔料厚と角膜上皮障害の関係を検討する目的で，黒色顔料をレンズ前面に格子状に印刷することで，顔料厚が異なる試作カラー CL 3種を作製した。顔料厚は，A<B<C の順に厚くした。これらカラー CL の各々3枚と，素材，含水率，直径，ベースカーブ，度数が試作レンズと同じ市販のレンズ3枚を，全身麻酔下で白色家兎12匹12眼に装用させ，眼瞼を縫合し72時間連続装用させた。72時間後に開瞼してレンズを外し，フルオレセイン染色をして細隙灯顕微鏡で角膜上皮障害の程度を観察した。市販レンズとレンズ A 装用眼では，中央角膜に軽度の点状表層角膜炎を認めた。レンズ B 装用眼では，点状表層角膜炎や角膜びらんを認めた。レンズ C では，3眼とも角膜びらんを認め，多発している個体があった。カラー CL では，印刷顔料厚の違いが角膜上皮障害発生に関係し，その厚さに依存して角膜上皮障害は重症化する。 （日コレ誌 56：294−297，2014）

キーワード：カラーコンタクトレンズ，顔料厚，角膜上皮障害

We studied the relationship between the thickness of the layer of color printed on cosmetic tinted contact lenses (Cos-CLs) and corneal epithelial disorders caused by Cos-CL wear. The study involved 12 New Zealand White rabbits (12 eyes) and 3 types of trial Cos-CLs (labeled A, B and C) printed with carbon-based black colorant. The layer of colorant was thinnest on lens A, thicker on lens B, and thickest on lens C. With the rabbits under general anesthesia, we placed trial lens A, B or C or a commercially available lens (made of the same material as the trial lenses and serving as the control) in each of 3 eyes and closed the eyes by tarsorrhaphy. After 3 days, we examined the corneas with fluorescein staining. In the 6 eyes wearing the control lens or trial lens A, we saw punctate keratitis. In the 3 eyes wearing trial lens B, we saw small corneal erosions and superficial punctate keratitis. In the 3 eyes wearing trial lens C, we saw large corneal erosions or multiple corneal erosions. In this study, the thickness of the colored layer was associated with the occurrence of corneal epithelial disorder, and the corneal epithelial disorder was more severe in eyes wearing lenses with thicker layers of colorant. (J Jpn CL Soc 56：294−297，2014)

Key Words : Cosmetic Tinted Contact Lens, Thickness of Colorants, Corneal Epithelial Disorder

緒 言

美容目的のカラーコンタクトレンズ（cosmetic tinted contact lens 以下 カラー CL）は，アジアの若年女性を中心に普及しており，近年はカラー CL 装用に関連した角膜障害が増加している[1-5]。カラー CL の素材は，比較的，酸素透過係数（Dk 値）が低い poly (hydroxyethyl methacrylate)（2-ヒドロキシエチルメタクリレート .以下 p-HEMA）であるものが多い上，着色部位の酸素透過率（Dk/L）は，理論的には透明部位より低下していると推察される。酸素透過率が低ければ，レンズ装用に伴う角膜上皮での低酸素から角膜上皮浮腫を来す。顔料着色によってレンズの剛性は変化するはずであり，剛性が変化したレンズは，角膜との摩擦を生む。ゆえに，カラー CL は通常の透明なソフト

別刷請求先：770-8503 徳島市蔵本町3-18-15 徳島大学大学院ヘルスバイオサイエンス研究部眼科学分野 江口 洋
Reprint requests to : Hiroshi Eguchi, MD Dept of Ophthalmol, Institute of Health Biosciences, The Univ of Tokushima Graduate School 3-18-15, Kuramoto-cho, Tokushima 770-8503, Japan

コンタクトレンズ（以下　SCL）よりも角膜上皮障害を誘発しやすいレンズと推察される。またカラーCLに着色された顔料が，レンズ表面かつ角膜側に印刷されている製品では，装用時に生じる印刷顔料による摩擦も，角膜上皮障害の発症に関係することが推測される。よってカラーCLでは，印刷顔料の厚みの違いによって，角膜上皮障害の程度に差が生じるとの仮説が成り立つが，これまでカラーCLでの印刷顔料厚による角膜上皮障害発生状況に差があるかどうかは検討がなされていない。そこで本研究は，カラーCL印刷顔料厚の違いが角膜上皮障害発生に影響を及ぼすかどうかを検証する目的で実施した。

実験対象ならびに方法

1．対　象

12カ月齢で体重2.4～2.6kgの白色家兎（New Zealand White）12匹12眼を実験対象とし，徳島大学大学院ヘルスバイオサイエンス研究部総合研究支援センター動物資源研究部門における動物実験委員会の承認（徳13098号）の下，日本学術会議による「動物実験の適正な実施に向けたガイドライン（2006年）」に遵守して実施された。

2．使用レンズ

p-HEMA製，含水率38％，直径14.0mm，ベースカーブ8.70mm，度数0ジオプターの試作カラーCL 3種類（A，B，C）および対照として，素材，直径，含水率，度数が試作レンズと同じSCL（シード1day Fine，株式会社シード社製）を準備した。試作カラーCLの印刷には，黒色顔料として市販のカラーCLでも使用されているカーボンブラックを使用し，格子状模様でパット印刷法によって印刷し，レンズA，B，およびCの順に1回，2回，および3回，同じ模様を上から重ねて印刷し，顔料厚をA，B，およびCの順に厚くした。各々のレンズの印刷顔料厚は，原子間力顕微鏡（VN-8000，株式会社キーエンス社製）を用いて，非印刷部と印刷部との平均的な高さの差を測定して算出した。レンズの詳細は，肉眼像や光学顕微鏡像を含め，図1～3に示す。

3．実験方法

全身麻酔（ケタミン20mg/kgとキシラジン2mg/kg混合液の筋肉注射）後の白色家兎の片眼の瞬膜を切除し，対照レンズと試作レンズA，B，Cを装用させ，4-0絹糸で眼瞼縁を2糸縫合し，72時間連続装用させた。装用後は，自力で開瞼してレンズが脱落していないかを日々確認し，途中でレンズが脱落した個体は実験対象から除外した。各レンズとも，72時間連続装用できていた3匹3眼（合計12匹12眼）で，72時間後に絹糸を切糸して開瞼し，オキシブプロカイン塩酸塩点眼後に無鉤鑷子で角膜を触ることなくレンズを外した後に，フルオレセイン染色をして細隙灯顕微鏡で角膜を観察した。

結　果

1．対照レンズ装用眼：3眼とも中央角膜に点状表層角膜炎や，線状の角膜上皮障害を来していた（図4A，B）が，角膜びらんを来した個体はなかった。
2．レンズA装用眼：3眼とも中央角膜に点状表層角膜炎や線状の角膜上皮障害があり，対照レンズ装用眼と同等であった（図5A，B）。
3．レンズB装用眼：3眼中2眼の角膜傍中心部に，楕円形の比較的大きな角膜びらんが1個生じていた（図6A，B）。ほかの1眼は点状表層角膜炎や線状の角膜上皮障害を生じていた。
4．レンズC装用眼：3眼すべてで角膜傍中心部に類円形の大きな角膜びらんが生じており，2眼では複数生じていた（図7A，B）。

考　按

今回の結果では，角膜側に顔料が印刷されたカラーCL

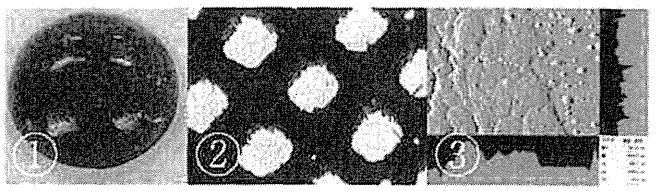

図1　レンズAの①肉眼像，②光学顕微鏡像，③原子間力顕微鏡像
①：黒色系の顔料が格子状に印刷されている。
②：白色部位が非印刷部をあらわす。
③：角膜側の顔料の最高点と非印刷部との最大高低差は504.6nmである。

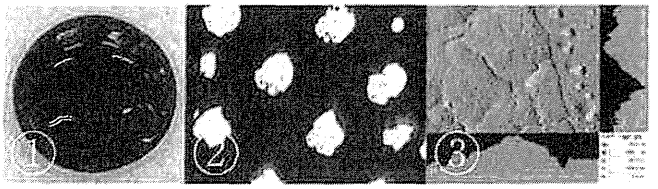

図2　レンズBの①肉眼像，②光学顕微鏡像，③原子間力顕微鏡像
①②：格子状模様が一度上塗りされ，レンズAより黒色部の面積が広くみえる。
③：顔料の最高点と非印刷部との最大高低差は932.8nmである。

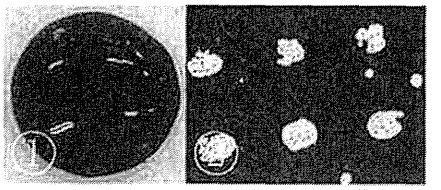

図3　レンズCの①肉眼像，②光学顕微鏡像
①②：格子状模様が二度上塗りされ，レンズA，Bより黒色部の面積が広くみえる。
顔料最高到達点は，原子間力顕微鏡の測定限界をこえていた。

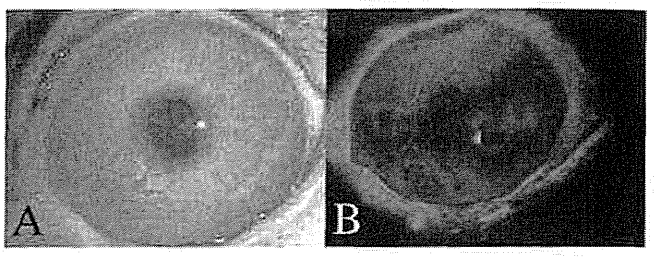

図4 対照レンズ装用眼のA 前眼部写真，B フルオレセイン染色像
A：結膜充血はほとんどない。
B：角膜上皮障害はわずかである。

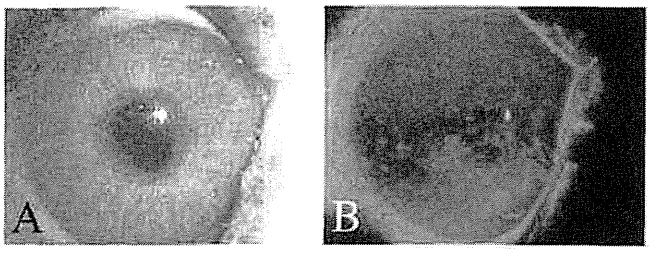

図5 レンズA装用眼のA 前眼部写真，B フルオレセイン染色像
A：結膜充血はほとんどない。
B：対照レンズ装用眼も同様で，角膜上皮障害はわずかである。

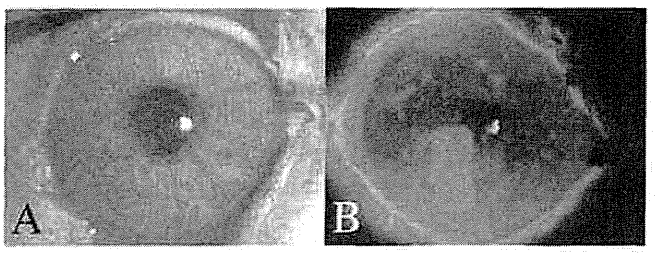

図6 レンズB装用眼のA 前眼部写真，B フルオレセイン染色像
A：結膜充血はほとんどない。
B：角膜傍中心部に楕円形のびらんがある。

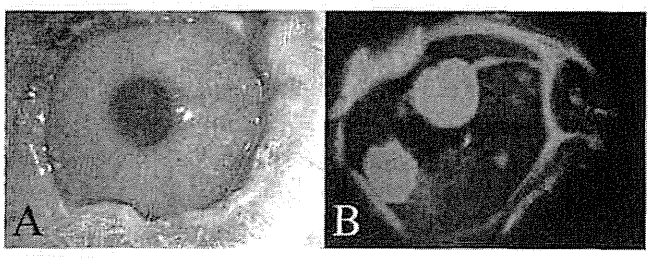

図7 レンズC装用眼のA 前眼部写真，B フルオレセイン染色像
A：結膜充血はほとんどない。
B：角膜傍中心部に円形のびらんが多発している。

では，顔料厚が厚くなるほど角膜上皮障害の程度が強くなった。よって，印刷顔料が厚いことは，カラーCLによる角膜障害の重要な危険因子であるといえる。これは，印刷顔料の厚みが厚くなるほど，印刷部の剛性が高くなることが原因だと思われる。印刷顔料厚が504.6nmであったレンズA装用眼は，顔料が印刷されていない対照レンズ装用眼と，角膜上皮障害の程度が同程度であったことから，顔料の厚さが500nm以内であれば，レンズの角膜側に印刷顔料が付着していても，角膜びらんを誘発しない可能性が示唆された。しかし，市販されているカラーCLにおいて，印刷顔料厚の情報は公開されていない。そもそも，印刷顔料がレンズのどちら側に，どのように印刷されているか，その成分も含め，実情は詳細に公開されているわけではない。したがって，眼科医にとって現時点で流通しているカラーCLの安全性を正確に評価することは困難であり，一般CL装用者には，それを判断することは不可能といえる。今後は，顔料厚を含めたカラーCLの印刷顔料の詳細な情報を精査し，安全なレンズの存在を確認した後，国民に啓発する必要がある。

CL装用に関連した角膜障害のなかで，最も避けるべき重篤な合併症は，感染性角膜炎である。岩崎ら[6]は，カラーCL装用に関連した点状表層角膜炎やcontact lens-induced acute red eye（以下 CLARE）様症例を報告しているが，CLAREは緑膿菌やセラチア属による急性炎症を示唆するとの報告[7]がある。レンズの素材や表面構造が，コンタクトレンズ（以下 CL）への細菌の付着や細菌性角膜炎の発症に影響することが知られている[8-11]。また，レンズ保存ケースは，CL関連細菌性角膜炎の起炎菌を保菌していることが分子生物学的に証明されている[12]。以上から，粗悪なケアをしながら，印刷顔料厚の厚いカラーCLを連日装用すれば，いずれは角膜上皮障害から感染性角膜炎を発症する可能性が高いと推察できる。更に，CL関連感染性角膜炎の起炎菌として最も多く分離される緑膿菌では，レンズ表面でバイオフィルムを産生しているとの報告[13,14]もある。印刷顔料厚が厚くなれば，レンズの表面積が広くなる。バイオフィルムは，様々な種の細菌が主として固形の生体材料に形成する。バイオフィルムと顔料成分との関係が不明なため断言は難しいが，印刷顔料厚が厚い製品では，細菌によるバイオフィルム汚染の危険が高いかもしれない。

本研究では，細隙灯顕微鏡で点状表層角膜炎と角膜びらんの有無のみを判定することで角膜上皮障害とカラーCL印刷顔料厚との関係を調べており，それら角膜所見の程度や，ほかの前眼部炎症所見との関係は調べられていない。当初は家兎眼を自然開瞼のまま毎日観察し，角膜上皮障害の程度だけでなく，充血や眼脂の程度をスコア化して比較検討する予定であった。しかし，瞬膜を切除していても自然開瞼してレンズが脱落する個体が相次いだため，眼瞼縫合で連続装用させるに至った。その結果，72時間・閉瞼状態での連続装用という，通常のCL装用者が装用しているよりも過酷な条件で観察することにした。しかし，すべての家兎の結膜充血は軽度であり，その所見にレンズ間の差

はなかった。同様に，眼脂もすべての眼でわずかしか出現しておらず，結膜充血や眼脂の程度は評価対象から外すこととした。結果的に，今回試作したカラーCLや対照として用いたレンズを家兎に3日間連続装用をしても，強い眼瞼炎や結膜炎を来すことはないことが判明した。しかし，あくまで家兎眼の72時間連続装用の結果であり，必ずしも人眼にあてはまるものではない。通常の装用条件における家兎眼での同様の検討も必要である。また，細隙灯顕微鏡所見では判別できない微細な炎症反応は，涙液の炎症性サイトカイン濃度の推移で判別できる可能性もあり[15]，今後は，同実験系での家兎涙液炎症性サイトカイン濃度の推移を検討する価値があると考えている。更に，カラーCL装用に伴う感染性角膜炎発症の危険因子を同定するためにも，感染症発症を誘発する因子を加味した後，結膜充血や眼脂の量を評価基準に加えることで，より詳細な検討が必要と思われる。

結論として，カラーCLでは，印刷顔料厚が厚いことが角膜上皮障害発生の危険因子であり，顔料の厚みに依存して角膜上皮障害が重篤になることが判明した。今後は，細隙灯顕微鏡では判別できない微細なレベルの炎症反応や，感染症発症要因を負荷した検証をすることで，カラーCL関連角膜炎発症の危険因子を，より詳細に検証する必要がある。

謝　辞

本研究の一部は，厚生労働科学研究費補助金医薬品・医療機器等レギュラトリーサイエンス総合研究事業「アカントアメーバ角膜炎制御にむけたコンタクトレンズケアの実態調査」（H25-医薬-指定-010）の分担研究として行われた。

文　献

1）Singh S, Satani D, Patel A & Vhankade R : Colored cosmetic contact lenses : An unsafe trend in the younger generation. Cornea 31 : 777-779, 2012.
2）Sauer A, Bourcier T & French Study Group for Contact Lenses Related Microbiol Keratitis : Microbial keratitis as a foreseeable complication of cosmetic contact lenses : A prospective study. Acta Ophthalmol 89 : e439-e442, 2011.
3）Spiteri N, Choudhary A & Kaye S : Pigmentation of the cornea secondary to tinted soft contact lens wear. Case Rep Ophthalmol Med 2012 : 852304, 2012. doi : 10.1155/2012/852304 [published Online First : 30 January 2012.]
4）Choi HW, Moon SW, Nam KH & Chung SH : Late-onset interface inflammation associated with wearing cosmetic contact lenses 18 months after laser in situ keratomileusis. Cornea 27 : 252-254, 2008.
5）Ray M & Lim DK : A rare polymicrobial keratitis involving *Chryseobacterium meningosepticum* and *Delftia acidovorans* in a cosmetic contact lens wearer. Eye & Contact Lens 39 : 192-193, 2013.
6）岩崎直樹，植田喜一，澤　充：カラーコンタクトレンズの眼障害を考える～カラーコンタクトレンズの諸問題の理解に向けて～．日コレ誌 55（補）：S7-S11，2013.
7）Holden BA, La Hood D, Grant T, Newton-Howes J et al : Gram-negative bacteria can induce contct lens related acute red eye (CLARE) response. CLAO J 22 : 47-52, 1996.
8）Giraldez MJ, Resua CG, Oliveira ME, Magariños B et al : Contact lens hydrophobicity and roughness effects on bacterial adhesion. Optom Vis Sci 87 : E426-431, 2010. doi : 10.1097/OPX.0b013e3183da8656.
9）Dart JK, Radford CF, Minassian D, Verma S et al : Risk factors for microbial keratitis with contemporary contact lenses : A case-control study. Ophthalmology 115 : 1647-1654, 2008.
10）Keay L, Edwards K, Naduvilath T, Forde K et al : Factors affecting the morbidity of contact lens-related microbial keratitis : A population study. Invest Ophthalmol Vis Sci 47 : 4302-4308, 2006.
11）Santos L, Rodrigues D, Lira M, Oliveira ME et al : The influence of surface treatment on hydrophobicity, protein adsorption and microbial colonisation of silicone hydrogel contact lenses. Cont Lens Anterior Eye 30 : 183-188, 2007.
12）Ogushi Y, Eguchi H, Kuwahara T, Hayabuchi N et al : Molecular genetic investigations of contaminated contact lens storage cases as reservoirs of *Pseudomonas aeruginosa* keratitis. Jpn J Ophthalmol 54 : 550-554, 2010.
13）Szczotka-Flynn LB, Imamura Y, Chandra J, Yu C et al : Increased resistance of contact lens-related bacterial biofilms to antimicrobial activity of soft contact lens care solutions. Cornea 28 : 18-26, 2009.
14）McLaughin-Borlace L, Stapleton F, Matheson M & Dart JKG : Bacterial biofilm on contact lens and lens storage cases in wearers with microbial keratitis. J Appl Microbiol 84 : 827-837, 1998.
15）Thakur A & Willcox MD : Cytokine and lipid inflammatory mediator profile of human tears during contact lens associated inflammatory disease. Exp Eye Res 67 : 9-19, 1998.

（2014年3月14日受付）

筆頭著者
江口　洋
徳島大学大学院ヘルスバイオサイエンス研究部眼科学分野

Brief Report

Landolt Ring-Shaped Epithelial Keratopathy
A Novel Clinical Entity of the Cornea

Tomoyuki Inoue, MD; Naoyuki Maeda, MD; Xiaodong Zheng, MD; Takashi Suzuki, MD; Daikichi Mitsuyama, MD; Norio Okamoto, MD; Tomoko Miura, MD; Tomiya Mano, MD; Yuichi Ohashi, MD

IMPORTANCE Landolt ring-shaped epithelial keratopathy is a newly identified disease with vesicular changes of unknown origin in the epithelial cells.

OBSERVATIONS Eleven Japanese patients with specific epithelial lesions that resembled a Landolt ring in the corneal epithelium were assessed. The main symptoms of Landolt ring-shaped epithelial keratopathy are foreign-body sensation and photophobia. Slitlamp examination indicates that Landolt ring-shaped lesions located only in the corneal epithelium are randomly distributed and occur unilaterally, bilaterally, or asymmetrically. Small lesions are sometimes connected to each other to form a large Landolt ring in a fractal pattern. Confocal microscopy reveals that the Landolt ring lesions are vesicular changes in the epithelial cells from the basal cell layer to the superficial cell layer without inflammation. The lesions form for weeks to months with sporadic exacerbations and natural remissions with or without treatments. The outcomes do not include epithelial disorders in the affected corneas or visual disruptions.

CONCLUSIONS AND RELEVANCE We describe a new disease entity of unknown origin referred to as Landolt ring-shaped epithelial keratopathy, which is usually bilateral and characterized by specific Landolt ring-shaped focal epithelial lesions with vesicular changes only in the epithelial cells. The disorder has an insidious onset and self-limiting nature despite treatment and should be included in the differential diagnosis of corneal epithelial disorders.

JAMA Ophthalmol. 2015;133(1):89-92. doi:10.1001/jamaophthalmol.2014.2381
Published online October 9, 2014.

Supplemental content at jamaophthalmology.com

Author Affiliations: Department of Ophthalmology, Ehime University School of Medicine, Ehime, Japan (Inoue, Zheng, Suzuki, Ohashi); Department of Ophthalmology, Osaka University Medical School, Osaka, Japan (Maeda); Mitsuyama Eye Clinic, Kanagawa, Japan (Mitsuyama); Okamoto Eye Clinic, Osaka, Japan (Okamoto); Okubo Ophthalmological Clinic, Suzaka Branch Hospital, Nagano, Japan (Miura); Tane Memorial Eye Hospital, Osaka, Japan (Mano).

Corresponding Author: Tomoyuki Inoue, MD, Department of Ophthalmology, Ehime University School of Medicine, Shitsukawa, Toon-City, Ehime, 791-0295, Japan (tomonoue@m.ehime-u.ac.jp).

The Landolt ring, a characteristic standardized symbol used to measure visual acuity (VA) in the daily outpatient clinic, is a ring with a gap that resembles the letter C (**Figure 1A**).[1] We describe 11 Japanese patients with specific epithelial lesions that resembled a Landolt ring in the corneal epithelium (Figure 1B). The institutional review board of Ehime University approved this study. All patients provided oral informed consent.

Report of Cases

Patient profiles are provided in eTable 1 in the Supplement. The patients were unrelated and not from the same hometown. The mean (SEM) patient age was 45.9 (5.3) years (age range, 17-73 years); 7 patients (64%) were in their 40s to early 50s. With bilateral disease (10 patients [91%]), the number of ring-shaped lesions differed between the eyes. The symptoms included a foreign-body sensation in 7 patients (64%), ocular pain in 5 patients (45%), or blurred vision in 4 patients (36%). Two patients (patients 2 and 3) had a history of dry eye, 2 (patients 5 and 9) had cataracts, 1 (patient 7) had allergic conjunctivitis, and 1 (patient 9) had glaucoma; 6 patients had no ocular complications before diagnosis. Regarding systemic disease, 2 patients (patients 4 and 5) had a history of cancer treatment, 1 (patient 1) had thyroid disease, and 1 (patient 6) had hepatitis and hypertension. No association was found with a systemic illness in any patients.

Clinical findings of the Landolt ring-shaped epithelial keratopathy are provided in eTable 2 in the Supplement. Eight patients initially had a VA of 20/20 or better; patients 5, 6, and 9 had VA in the worse affected eye below 20/20. The bilateral VA decrease in patients 5 and 9 resulted from cataracts. Only patient 6 had no ocular complications that led to decreased VA before disease onset. The intraocular pressure was not elevated in any patients. Slitlamp examination revealed the Landolt ring-shaped lesions in the corneal epithelium, which can be observed more easily with fluorescein staining (Figure 1). The Landolt ring-shaped lesions, which were randomly distributed on the cornea, were single or multiple in the diseased corneas and different sizes; the gap in the C shape was randomly located. The Landolt ring-shaped lesions appeared and disappeared over time with or without treatment. The lesions were unilateral, bilateral, or asymmetric. Although, in

Figure 1. The Landolt Ring

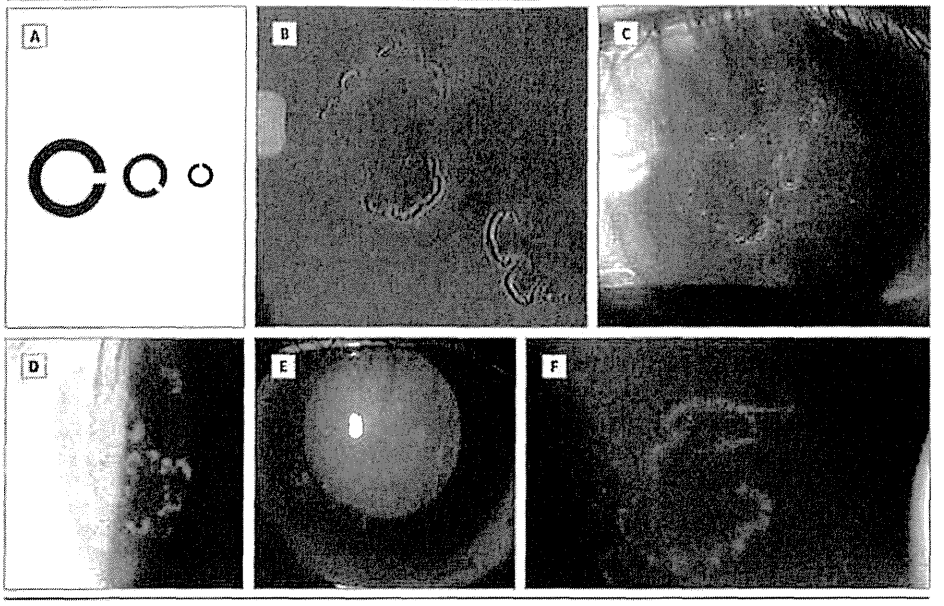

A, Schematic figure of a Landolt ring used during visual acuity examinations. The Landolt ring is incomplete, with a gap resembling the letter C. B, Slitlamp photograph with fluorescein staining obtained from patient 10 shows representative Landolt ring-shaped epithelial lesions. Slitlamp photographs with fluorescein staining from patients 9 (C), 8 (D), 5 (E), and 7 (F).

Figure 2. Fractal Patterns of Landolt Ring-Shaped Lesions

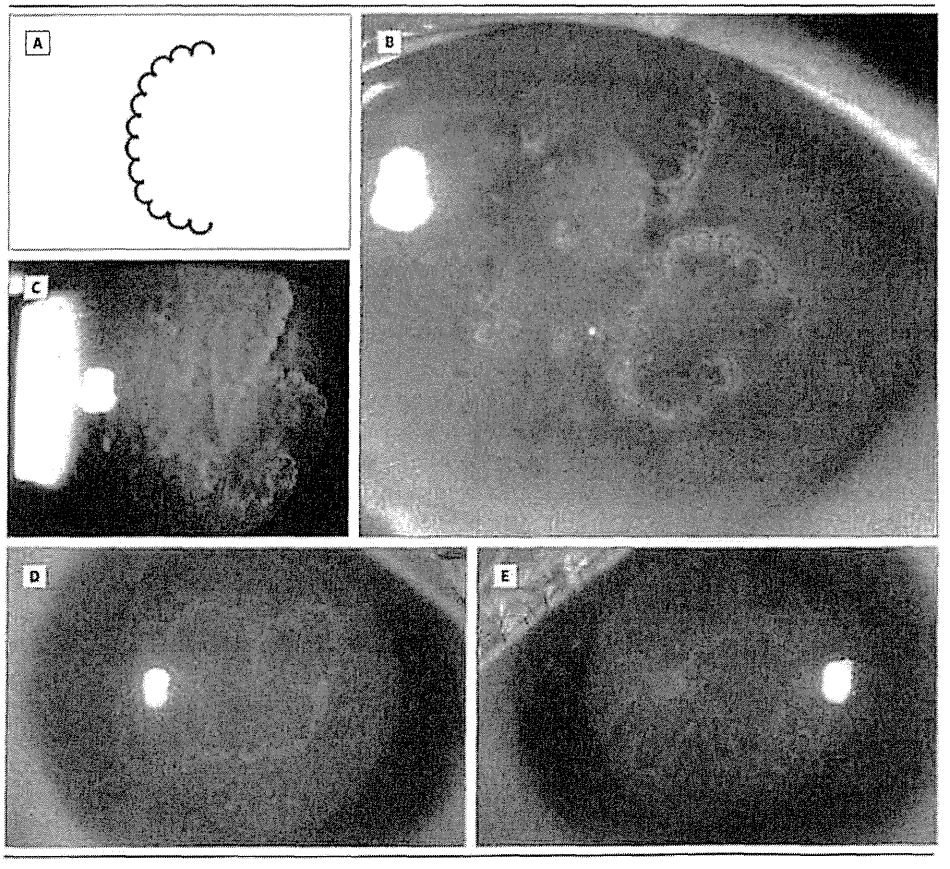

A, Schematic figure of a fractal pattern of the Landolt ring. Several small lesions are connected to each other to form a large Landolt ring. Large lesions with a fractal pattern form a large letter C seen by retroillumination (B) and fluorescein staining (C) in patient 4. Large lesions with a fractal pattern on a slitlamp photograph with fluorescein staining in patient 6 form large circular lesions in the right (D) and left (E) eyes when small Landolt rings became connected.

some cases, the Landolt lesions were independent of each other, several small lesions were connected to form a large Landolt ring (**Figure 2A**) in a fractal pattern, with a statistical similarity in form over a range of magnifications of many natural shapes, objects, and phenomena.[2-4] Figure 2 shows representative fractal lesions of Landolt ring-shaped epithelial keratopathy in patients 4 and 6.

The keratopathy was restricted to the epithelium in all patients, with no corneal infiltration, edema, or endothelial changes. No anterior chamber inflammation or keratic pre-

Figure 3. Slitlamp Photograph From Patient 1 Obtained by Various Forms of Illumination

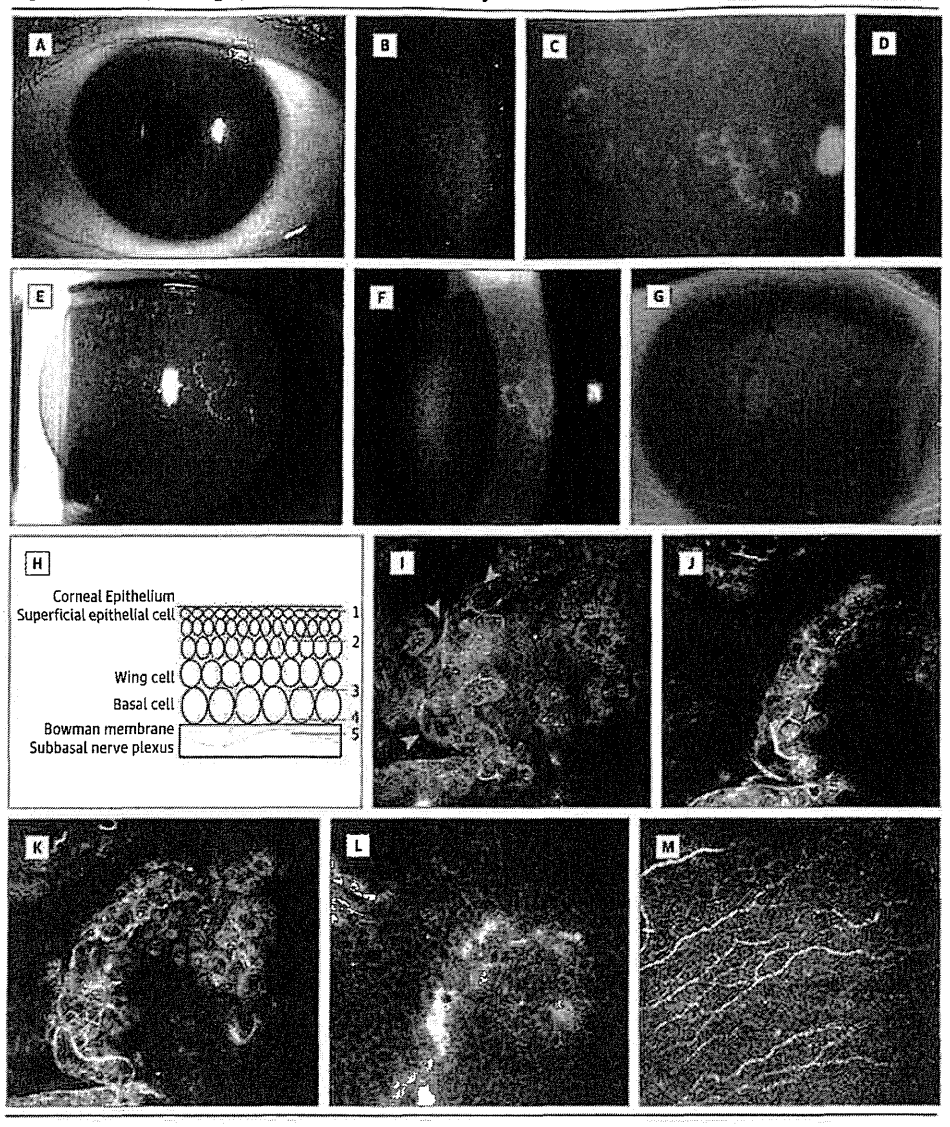

A, Diffuser illumination; B, broad slit illumination; C, fluorescein staining; D, thin slit illumination; E, retroillumination; F, broad slit illumination with fluorescein staining; and G, fluorescein staining. H, Schematic figure of the corneal epithelium and the Bowman membrane. I, Confocal image at the depth of the blue line (line 1) for superficial epithelial level scanning shows cellular ballooning and hyporeflective cytoplasmic changes (arrows). J, Confocal image at the depth of the blue line (line 2) for wing cell layer level scanning shows hyperreflective nuclear (arrow) and cell membranes. K, Confocal image at the depth of the blue line (line 3) for basal cell layer scanning shows ridge formation into the Landolt shape. L, Confocal image at the depth of the blue line (line 4) for the bottom level of the basal cell layer shows abnormal hyperreflective precipitates. M, Confocal image at the depth of the blue line (line 5) for the subbasal nerve plexus shows normal morphologic features.

cipitates were observed. No conjunctivitis was observed except in patient 7. The corneal sensitivity was measured using Cochet-Bonnet esthesiometry in patients 1, 2, 3, 4, 7, and 11; no decreased corneal sensitivities (60 mm) were observed. No funduscopy findings were apparent in any patients. Polymerase chain reaction was performed to detect human herpesvirus 1 to 8 DNA[5-7] on scraped corneal specimens and/or in tear samples from 6 patients (patients 1, 2, 3, 5, 7, and 11), of which results were negative for all patients.

The clinical course of the Landolt ring-shaped epithelial keratopathy is provided in eTable 3 in the Supplement. The Landolt ring-shaped lesions developed at clinical diagnosis in December in 5 patients (45%), March in 4 patients (36%), November in 1 patient (9%), and February in 1 patient (9%). The disease onset and resolution were within the first year after diagnosis. The periods of recurrence after the second year or later after the initial diagnosis were January to March of year 2 after diagnosis in patient 2; December to April of year 2 in patient 5; and December of year 2, November to May of year 3, and October to March of year 4 in patient 3. The months at onset of all 11 patients were October to March, and the periods during which the Landolt lesions were observed were October to June. The Landolt ring lesions tended to form in winter, especially with seasonal change. After development, the lesions gradually resolved (mean [SEM] time to resolution, 3.0 [0.6] months). The numbers and sizes of the Landolt ring lesions often repeatedly decreased and increased, and the severities varied during the disease course.

The slitlamp findings revealed that after lesion development, no epithelial disorders occurred in the affected corneas of any patients (**Figure 3**). No patients reported a visual disturbance, foreign-body sensation, or eye pain at the final examination. Landolt ring-shaped lesions recurred in 3 patients (27%) during the follow-up period. The mean (SEM) follow-up period from detection of this epithelial keratopathy was 11.0 (5.3) months (range, 2 weeks to 54 months). Topical treatments included a corticosteroid agent for 5 patients (45%), an immunosuppressive agent for 1 patient (9%), an antiallergic

agent for 3 patients (27%), an antimicrobial agent for 5 patients (45%), artificial tears for 2 patients (18%), and an antiherpetic agent for 1 patient (9%). Two patients (18%) were untreated.

To obtain more detailed lesion characterization at the cellular level, in vivo confocal microscopy using the Heidelberg Retinal Tomograph II Rostock Cornea Module (Heidelberg Engineering)[8,9] was performed. Figure 3I-M shows representative images of the Landolt ring-shaped lesions in patient 1. Superficial epithelial layer scanning revealed cellular ballooning and hyporeflective cytoplasmic changes (Figure 3I). Wing cell level scanning revealed hyperreflective nuclear and cell membranes (Figure 3J). Basal cell layer level scanning revealed ridge formation into the Landolt ring (Figure 3K). The bottom level of the basal cells had abnormal hyperreflective precipitates (Figure 3L). At the Bowman layer, the subbasal nerve plexus had normal morphologic features (Figure 3M). The long nerve fibers ran parallel to the Bowman layer.[10] These findings indicate that the Landolt ring-shaped lesions formed as a result of morphologic changes; vesicular cellular ballooning in the basal cells was continuous with the superficial cellular layer only within the epithelial layer. Fluorescein staining of the Landolt ring-shaped lesions did not reveal epithelial erosion but revealed disruption of the epithelial junction from swelling of the epithelial cellular surface caused by serial cellular ballooning from the basal cell layer. The corneal stromal layer was normal without activated keratinocytes with highly reflective cellular bodies; the endothelial layer was normal. No Langerhans cells were seen around the lesions.

Discussion

We propose a new disease entity called Landolt ring-shaped epithelial keratopathy. Our 11 patients had interesting disease characteristics. This disease of unknown origin was usually chronic, bilateral, and characterized by a specific focal epithelial lesion that resembled the letter C and was composed of vesicular changes in the epithelial cell layer without apparent inflammation. The lesions often continued to appear for weeks to months with sporadic exacerbation and natural remission. Landolt ring disease differed from other previously described corneal epithelial disorders.[11-15] Although the current study described 11 Japanese patients with Landolt ring-shaped epithelial keratopathy, it is unclear whether this is relevant only to a Japanese population or worldwide. To our knowledge, no other patients currently have this condition. If this report draws worldwide attention to this disease, more information about its distribution may later be revealed. Genetic studies may be useful to clarify the features. The origin of Landolt ring-shaped corneal epitheliopathy is unknown, and further investigation is needed.

ARTICLE INFORMATION

Submitted for Publication: December 8, 2014; final revision received April 7, 2014; accepted April 8, 2014.

Published Online: October 9, 2014. doi:10.1001/jamaophthalmol.2014.2381.

Author Contributions: Dr Inoue had full access to all the data in this study and takes responsibility for the integrity of the data and the accuracy of the data analysis.
Study concept and design: Inoue, Ohashi.
Acquisition, analysis, or interpretation of data: All authors.
Drafting of the manuscript: Inoue, Zheng, Suzuki, Mitsuyama, Okamoto, Miura, Mano.
Critical revision of the manuscript for important intellectual content: Maeda, Ohashi.
Administrative, technical, or material support: Inoue, Maeda, Suzuki, Mitsuyama, Okamoto, Miura, Mano.
Study supervision: Maeda, Ohashi.

Conflict of Interest Disclosures: All authors have completed and submitted the ICMJE Form for Disclosure of Potential Conflicts of Interest and none were reported.

REFERENCES

1. Duke-Elder S, ed. *System of Ophthalmology.* Vol V. London, England: Henry Kimptom; 1970:426-427.
2. Mandelbrot B. How long is the coast of Britain? statistical self-similarity and fractional dimension. *Science.* 1967;156(3775):636-638.
3. Montague PR, Friedlander MJ. Expression of an intrinsic growth strategy by mammalian retinal neurons. *Proc Natl Acad Sci U S A.* 1989;86(18):7223-7227.
4. Landini G, Mission GP, Murray PI. Fractal properties of herpes simplex dendritic keratitis. *Cornea.* 1992;11(6):510-514.
5. Inoue T, Kandori M, Takamatsu F, Hori Y, Maeda N. Corneal endotheliitis with quantitative polymerase chain reaction positive for human herpesvirus 7. *Arch Ophthalmol.* 2010;128(4):502-503.
6. Inoue T, Takamatsu F, Kubota A, Hori Y, Maeda N, Nishida K. Human herpesvirus 8 in corneal endotheliitis resulting in graft failure after penetrating keratoplasty refractory to allograft rejection therapy. *Arch Ophthalmol.* 2011;129(12):1629-1630.
7. Inoue T, Kawashima R, Suzuki T, Ohashi Y. Real-time polymerase chain reaction for diagnosing acyclovir-resistant herpetic keratitis based on changes in viral DNA copy number before and after treatment. *Arch Ophthalmol.* 2012;130(11):1462-1464.
8. Patel DV, McGhee CN. In vivo confocal microscopy of human corneal nerves in health, in ocular and systemic disease, and following corneal surgery: a review. *Br J Ophthalmol.* 2009;93(7):853-860.
9. Guthoff RF, Zhivov A, Stachs O. In vivo confocal microscopy, an inner vision of the cornea: a major review. *Clin Experiment Ophthalmol.* 2009;37(1):100-117.
10. Zheng X, Shiraishi A, Okuma S, et al. In vivo confocal microscopic evidence of keratopathy in patients with pseudoexfoliation syndrome. *Invest Ophthalmol Vis Sci.* 2011;52(3):1755-1761.
11. Burstein NL. Corneal cytotoxicity of topically applied drugs, vehicles and preservatives. *Surv Ophthalmol.* 1980;25(1):15-30.
12. Stocker FW, Holt LB. Rare form of hereditary epithelial dystrophy of the cornea: genetic, clinical, and pathologic study. *AMA Arch Ophthalmol.* 1954;53(4):536-541.
13. Kenyon KR. Recurrent corneal erosion: pathogenesis and therapy. *Int Ophthalmol Clin.* 1979;19(2):169-195.
14. Cook SD. Herpes simplex virus in the eye. *Br J Ophthalmol.* 1992;76(6):365-366.
15. Tabbara KF, Ostler HB, Dawson C, Oh J. Thygeson's superficial punctate keratitis. *Ophthalmology.* 1981;88(1):75-77.

JCM
Journals.ASM.org

Development of an Immunochromatographic Assay Kit Using Fluorescent Silica Nanoparticles for Rapid Diagnosis of *Acanthamoeba* Keratitis

Koji Toriyama,[a] Takashi Suzuki,[a] Tomoyuki Inoue,[a] Hiroshi Eguchi,[b] Saichi Hoshi,[c] Yoshitsugu Inoue,[d] Hideki Aizawa,[e] Kazutomi Miyoshi,[e] Michio Ohkubo,[e] Eiji Hiwatashi,[f] Hiroshi Tachibana,[g] Yuichi Ohashi[a]

Department of Ophthalmology, Ehime University, Graduate School of Medicine, Ehime, Japan[a]; Department of Ophthalmology, Institute of Health Biosciences, University of Tokushima Graduate School, Tokushima, Japan[b]; Fujieda Municipal General Hospital, Shizuoka, Japan[c]; Division of Ophthalmology and Visual Science, Faculty of Medicine, Tottori University, Tottori, Japan[d]; Furukawa Electric Co., Ltd., Tokyo, Japan[e]; Department of Ophthalmology, Ofuna Chuo Hospital, Kanagawa, Japan[f]; Department of Infectious Diseases, Tokai University School of Medicine, Kanagawa, Japan[g]

We developed an immunochromatographic assay kit that uses fluorescent silica nanoparticles bound to anti-*Acanthamoeba* antibodies (fluorescent immunochromatographic assay [FICGA]) and evaluated its efficacy for the detection of *Acanthamoeba* and diagnosis of *Acanthamoeba* keratitis (AK). The sensitivity of the FICGA kit was evaluated using samples of *Acanthamoeba* trophozoites and cysts diluted to various concentrations. A conventional immunochromatographic assay kit with latex labels (LICGA) was also evaluated to determine its sensitivity in detecting *Acanthamoeba* trophozoites. To check for cross-reactivity, the FICGA was performed by using samples of other common causative pathogens of infectious keratitis, such as *Pseudomonas aeruginosa*, *Staphylococcus aureus*, *Staphylococcus epidermidis*, and *Candida albicans*. Corneal scrapings from patients with suspected AK were tested with the FICGA kit to detect the presence of *Acanthamoeba*, and the results were compared with those of real-time PCR. The FICGA kit detected organisms at concentrations as low as 5 trophozoites or 40 cysts per sample. There were no cross-reactivities with other pathogens. The FICGA was approximately 20 times more sensitive than the LICGA for the detection of *Acanthamoeba* trophozoites. The FICGA kit yielded positive results for all 10 patients, which corresponded well with the real-time PCR results. The FICGA kit demonstrated high sensitivity for the detection of *Acanthamoeba* and may be useful for the diagnosis of AK.

Acanthamoeba keratitis (AK) is a severe and sight-threatening ocular infection which usually occurs in the context of soft contact lens wear or trauma. It is caused by *Acanthamoeba* spp. which inhabit various environments, such as lakes, oceans, soil, and tap water (1–3). *Acanthamoeba* can assume two different morphological forms: the trophozoite, which can utilize nutrition and proliferate, and the dormant protective cyst, which can withstand high temperatures, desiccation, and pharmacologic insults. *Acanthamoeba* can transform between the trophozoite and cyst forms to adjust to various environments (3–6). The incidence of AK has increased dramatically in recent years, a trend which has been attributed to the increasing prevalence of soft contact lens wear and usage of contact lens disinfectant solutions that do not prevent the growth of *Acanthamoeba* (7, 8). Since the clinical manifestations of AK are similar to those of herpes simplex keratitis, the condition can often be misdiagnosed (9–11). Therefore, reliable detection of *Acanthamoeba* is essential for an accurate diagnosis of AK. As delayed diagnosis has been associated with poor visual outcomes (12, 13), it is important to identify a method for the rapid and specific diagnosis of AK.

Microscopic examination and culture of corneal scrapings are the diagnostic procedures conventionally used to detect *Acanthamoeba* (14). Microscopic examination of corneal smears stained with Fungiflora Y, calcofluor white stain, and acridine orange stain has been reported to be an effective method of diagnosing AK (15–17), but these tests require technical expertise, and a false negative can occur if there is an insufficient sample from the corneal scraping. Culturing live *Acanthamoeba* isolates is time-consuming, and a long incubation time is needed to confirm *Acanthamoeba* growth. This results in decreased sensitivity of the test and delays in starting treatment (14, 18).

Recently, highly sensitive PCR procedures which amplify *Acanthamoeba* DNA have been used in the diagnosis of AK (19–22). Real-time PCR can also provide quantitative values for *Acanthamoeba* DNA copy numbers, enabling clinicians to estimate the efficacy of AK treatment (23, 24). However, these genetic procedures require expensive specialized equipment and technical expertise. Moreover, these tests are available only in certain facilities, such as academic centers.

Immunochromatographic assays (ICGA) are useful for antigen detection, and they can generally be completed within 30 min and do not require specialized equipment or expertise (25–29). Because of its rapidity and simplicity, the ICGA is utilized in many clinical tests, such as pregnancy tests and tests which detect antigens from causative

Received 5 September 2014 Returned for modification 3 October 2014
Accepted 4 November 2014
Accepted manuscript posted online 12 November 2014
Citation Toriyama K, Suzuki T, Inoue T, Eguchi H, Hoshi S, Inoue Y, Aizawa H, Miyoshi K, Ohkubo M, Hiwatashi E, Tachibana H, Ohashi Y. 2015. Development of an immunochromatographic assay kit using fluorescent silica nanoparticles for rapid diagnosis of *Acanthamoeba* keratitis. J Clin Microbiol 53:273–277. doi:10.1128/JCM.02595-14.
Editor: N. A. Ledeboer
Address correspondence to Takashi Suzuki, t-suzuki@m.ehime-u.ac.jp.

doi:10.1128/JCM.02595-14

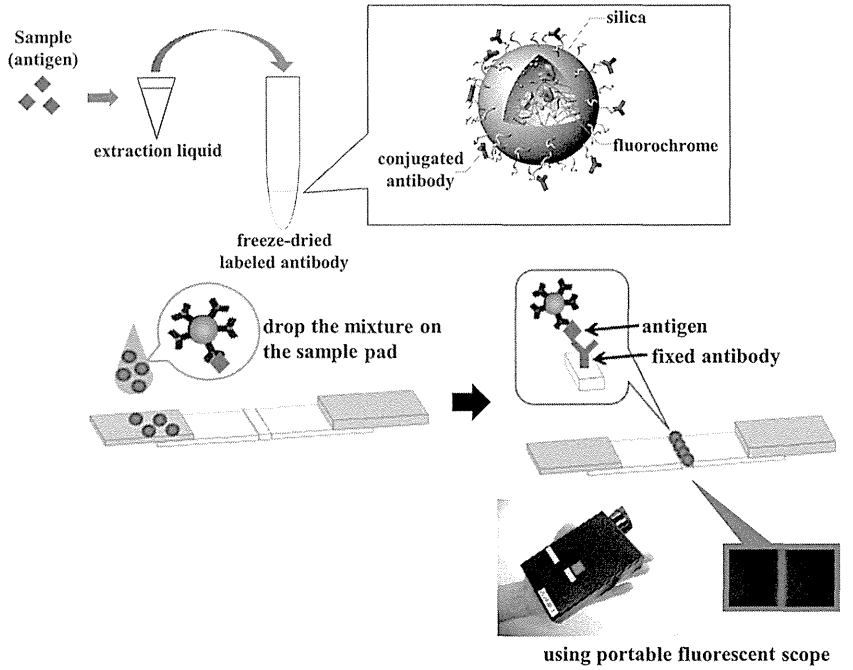

FIG 1 Principle of the fluorescent immunochromatographic assay kit. The sample is treated with extraction liquid and mixed with anti-*Acanthamoeba* monoclonal antibodies, which are conjugated to fluorescent silica nanoparticles. *Acanthamoeba* antigens, if present in the sample, form complexes with antibodies which are fixed in place on a strip. Fluorescent emission is observed by using a portable fluorescence microscope. If there are no *Acanthamoeba* antigens in the sample, no fluorescent band is observed.

pathogens, such as viruses and bacteria (25–27). In the field of ophthalmology, it is used for the diagnosis of adenoviral conjunctivitis and herpetic keratitis (28, 29). Colloidal gold and latex, each of which serves as a label when coupled to an antibody, are used to visualize antigens in ICGA kits for adenovirus and herpesvirus, respectively (28, 29). ICGA kits that use colloidal gold or latex labels usually show results using a detection line which appears on the membrane in either blue or red. However, checking for this detection line with only the naked eye is not ideal, as it may reduce the test's sensitivity or lead to false positives (30).

In this study, an ICGA kit using an anti-*Acanthamoeba* antibody was developed to detect *Acanthamoeba*. A fluorescent substance, instead of colloidal gold or latex, was used to label the anti-*Acanthamoeba* antibody, and the detection line was visualized using a portable fluorescence microscope. The ICGA kit used in this study (the fluorescent immunochromatographic assay [FICGA]) consists of a test strip, extraction liquid containing surfactant, and fluorescent silica nanoparticles (Quartz Dot; Furukawa Electric Co., Ltd.), each coupled with an antibody for *Acanthamoeba castellanii*. Quartz Dot is an amorphous silica nanoparticle with a diameter of approximately 290 nm and is harmless to the human body. Since the surface of the particle is covered by highly hydrophilic hydroxyl groups, the particles disperse uniformly in the sample solution or buffer. Nonspecific adsorption due to hydrophobic interactions is infrequent, thereby minimizing fluorescent noise and maximizing sensitivity. Moreover, the antibody-fluorescent label complex is stabilized by strong covalent modifications on its surface and has high luminance since it contains a high concentration of the fluorochrome rhodamine 6G. Rhodamine 6G is an ideal fluorescent marker because it fluoresces at 555 nm, a wavelength to which the eye is extremely sensitive under light-adapted conditions (31). We used mouse monoclonal antibodies to *Acanthamoeba castellanii*, which were produced as previously described (32). These antibodies recognize pathogenic *Acanthamoeba* spp. but not any other amoebas (32). The aim of this study was to investigate the efficacy of a FICGA for the detection of *Acanthamoeba* and diagnosis of AK.

MATERIALS AND METHODS

Immunochromatographic assay for detection of *Acanthamoeba*. To perform the assay, a sample was treated with 200 μl of extraction liquid and freeze-dried fluorescent silica nanoparticles, and 80 μl of this mixture was placed on the edge of a test strip which had been previously sprayed with anti-*Acanthamoeba* antibodies. Thirty minutes after applying the sample mixture, the fluorescent emission was observed with a portable fluorescence microscope (Immuno Chromato-Reader; Furukawa Electric Co., Ltd.) (Fig. 1). The fluorescent intensity of the test line was also measured with a specialized fluorescent scanner 60 min after application of the sample. The fluorescence microscope can detect signals at an intensity of approximately 100 arbitrary units.

A second ICGA kit was developed with the same mouse-derived anti-*Acanthamoeba* antibodies labeled with latex markers (the latex-labeled immunochromatographic assay [LICGA]). For this kit, equal parts of sample fluid and antibody solution were mixed, and 100 μl of this mixture was applied to a test strip with an anti-*Acanthamoeba* antibody test line and a mouse IgG control antibody line. The test result was confirmed within 30 min after sample application. A red band at both the test and control antibody line positions was considered a positive result, whereas a negative result consisted of a red band at the control position only.

***In vitro* examination.** *Acanthamoeba castellanii* strain ATCC 30011 was purchased from the American Type Culture Collection and used to examine the sensitivity of the FICGA and LICGA kits.

Trophozoites were grown axenically in peptone-yeast extract-glucose (PYG) medium at 25°C in a tissue culture flask (Becton Dickinson, Tokyo,

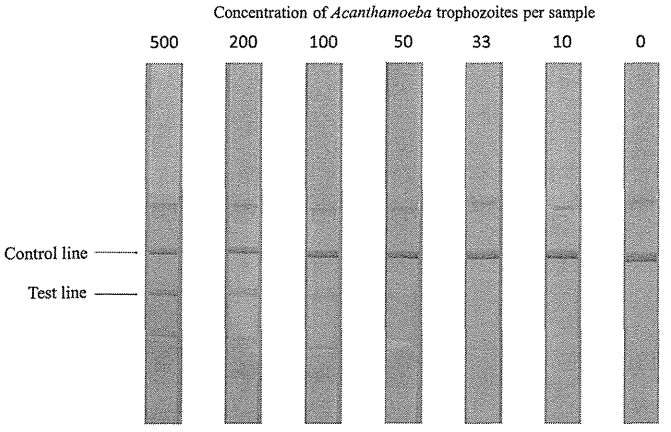

FIG 2 Photograph of test strips used for an immunochromatographic assay with latex labels. The *Acanthamoeba castellanii* concentration (number of trophozoites per sample) is shown above each strip. The test line was seen at concentrations of at least 100 trophozoites per sample.

Japan). Encystment was induced by transferring the trophozoites from the PYG medium to Neff's constant-pH encystment medium and incubating the trophozoites for at least 2 weeks at 25°C (33). The number of trophozoites or cysts in suspension was counted using a hemocytometer and diluted using extraction liquid.

For the LICGA, a diluted trophozoite culture was applied to the test strip, and the test line was checked for a reaction. Three independent assays were performed with different concentrations of *Acanthamoeba* solution. For the FICGA, culture media of trophozoites and cysts were applied to the FICGA kit. The test strips were evaluated for the presence or absence of fluorescence via microscopic examination. The fluorescent intensity of each test line was also measured to determine whether signal intensity was correlated with the *Acanthamoeba* concentration in the samples. In examinations with both the LICGA and the FICGA, the person assessing the positive or negative result was not informed of the *Acanthamoeba* concentration in the samples.

Cross-reactivity tests were conducted for *Pseudomonas aeruginosa* (strain PAO-1), *Staphylococcus aureus* (strain Newman), *Staphylococcus epidermidis* (clinical isolate), and *Candida albicans* (clinical isolate), which are common causative pathogens of infectious keratitis. The culture medium of each pathogen was diluted to a concentration of 10^7 CFU/ml using extraction liquid and then applied to the FICGA test strip.

Clinical evaluation. (i) Subjects and samples. Clinical samples were collected from 10 patients (5 men and 5 women, ranging from 18 to 57 years of age) with suspected AK based on the clinical presentation. In order to collect a sample, we scraped corneal lesions liberally to obtain a sufficient amount of tissue and to maximize the amount of *Acanthamoeba* collected. The samples were divided into equal parts for each of the following examinations: FICGA, real-time PCR for *Acanthamoeba* DNA, direct microscopic examination, and culture. In three cases where a sufficient amount of sample was not obtained, the samples were examined by only the FICGA and real-time PCR. All of these examinations were conducted by an investigator who was not involved in the care of the patients. Informed consent was obtained from each patient.

This study was approved by the institutional review board of Ehime University Hospital, and the procedures we performed followed the Declaration of Helsinki.

(ii) Microbial examination and real-time PCR. Scrapings were smeared onto glass slides, and some were Gram stained (in 6 cases) or stained with Fungiflora Y (in 1 case). The slides were examined by light and fluorescence microscopy. Samples were inoculated directly onto 1.5% nonnutrient agar (NNA) overlaid with *Escherichia coli* and cultured for at least 7 days at room temperature (25°C to 30°C). The samples were prepared for real-time PCR analysis for *Acanthamoeba* DNA as described previously (22).

TABLE 1 Detection of *Acanthamoeba* by fluorescent immunochromatographic assay

Morphological form	Result at an *Acanthamoeba* concentration (no. of organisms) of[a]:								
	0	5	8	10	20	40	80	800	8,000
Trophozoites	−	+	NT	+	+	+	+	+	NT
Cysts	−	NT	−	NT	−	+	+	+	+

[a] +, positive; −, negative; NT, not tested.

RESULTS

***In vitro* examination.** The aim of this study was to evaluate the sensitivity of the LICGA and the FICGA for the detection of *Acanthamoeba*. The thresholds for detecting *Acanthamoeba* trophozoites with the LICGA are shown in Fig. 2. Three independent assays showed similar results, namely, that trophozoites were detected via this method at concentrations of >100 trophozoites per sample. The thresholds for detecting *Acanthamoeba* trophozoites and cysts with the FICGA kit are shown in Table 1. The FICGA kit detected trophozoites at concentrations as low as 5 organisms per sample and cysts at concentrations as low as 40 organisms per sample. The FICGA was approximately 20 times more sensitive than the LICGA for detecting *Acanthamoeba* trophozoites. There was a strong positive correlation between the intensities of the fluorescent test lines (as measured by a specialized fluorescent scanner) and the *Acanthamoeba* concentrations in the trophozoite and cyst forms (Fig. 3).

When samples of *P. aeruginosa*, *S. aureus*, *S. epidermidis*, and *C. albicans* were used, the FICGA yielded negative results, and there were no cross-reactivities.

Clinical evaluation. Samples from all 10 patients tested positive for *Acanthamoeba* DNA when evaluated by real-time PCR (Table 2). The maximum copy number was 4.0×10^5 copies per sample, and the minimum was <25 copies per sample. The

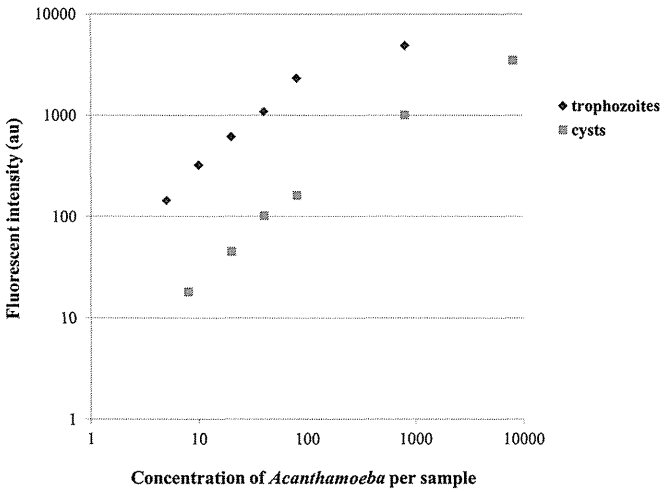

FIG 3 Correlation between fluorescent intensity of the test line measured by a specialized fluorescent scanner and concentration of *Acanthamoeba* trophozoites and cysts in the samples. There was a significant positive correlation between fluorescent intensity and the *Acanthamoeba* concentration in the trophozoite and cyst forms. au, arbitrary units.

TABLE 2 Profiles of patients and results of various diagnostic tests for *Acanthamoeba*

Case no.	Age (yr)	Sex[a]	Smear result	Culture result	Real-time PCR result (DNA copy no.)	FICGA result[b]
1	19	F	Negative[c]	Negative	Positive (1.1×10^5)	Positive
2	18	M	Negative[c]	Positive	Positive (6.8×10)	Positive
3	19	F	NT[d]	NT	Positive (1.2×10^5)	Positive
4	57	F	NT	NT	Positive (<25)	Positive
5	32	F	Negative[c]	Negative	Positive (1.0×10^2)	Positive
6	50	M	NT	NT	Positive (4.0×10^5)	Positive
7	24	F	Negative[c]	Negative	Positive (<25)	Positive
8	29	M	Positive[c]	Positive	Positive (2.5×10^4)	Positive
9	36	M	Positive[c]	Negative	Positive (2.3×10^3)	Positive
10	30	M	Positive[e]	Positive	Positive (3.2×10^4)	Positive

[a] M, male; F, female.
[b] FICGA, fluorescent immunochromatographic assay.
[c] Gram stain.
[d] NT, not tested.
[e] Fungiflora Y stain.

FICGA kit detected *Acanthamoeba* in all 10 patients, consistent with the results of real-time PCR. In 7 patients who were evaluated by smear analysis and culture, the smears and cultures were both positive in 2 patients. Either the culture or the smear was positive in 2 patients, and both studies were negative in the remaining 3 patients. All patients responded well to treatment with antiamoebic therapy with topical biguanides and antifungals.

DISCUSSION

In recent years, amplification of *Acanthamoeba* DNA by PCR has become the principal procedure for detecting *Acanthamoeba* and enabling sensitive diagnosis of AK (19–24). However, PCR has some limitations, as previously stated. A rapid and readily available procedure would help to ensure an accurate diagnosis at the first visit and reduce the risk of inappropriate treatments that complicate the clinical picture and make diagnosis more difficult. In the current study, we succeeded in developing an ICGA kit for detecting *Acanthamoeba* antigens. This kit was able to detect *Acanthamoeba* within just 30 min and was extremely simple to use compared with other diagnostic procedures. This test may enable clinicians to diagnose AK in the outpatient examination room. Although the ICGA is quick and easy to use, most existing kits have relatively low sensitivities. For instance, the sensitivity of the ICGA kit for detecting adenovirus has been reported as approximately 60%, whereas the specificity is >90% (29). In order to improve sensitivity, we used antibodies conjugated with fluorescent silica nanoparticles. In our novel FICGA kit, we examined the test line for the presence or absence of fluorescence using a portable fluorescence microscope. We expected that this detection method would be more sensitive than conventional ICGA tests, which are read by direct examination with the naked eye. Our current results demonstrate that the FICGA kit was 20 times more sensitive for detecting *Acanthamoeba* than the conventional LICGA kit, indicating that the FICGA is a promising approach for improving the accuracy of pathogen detection in a variety of infectious diseases. Although a specialized fluorescence microscope is required to read the test strips, it is a small device which is easy to acquire and is relatively inexpensive, and therefore it can be made available in nearly any local clinic.

In the *in vitro* portion of the examination, *Acanthamoeba* cysts were detected at concentrations as low as 40 organisms per sample, whereas trophozoites were detected at concentrations as low as 5 organisms per sample. It is unclear why the assay was less sensitive for detecting cysts than for detecting trophozoites, but one possibility is that unlike trophozoites, cysts may not reliably lyse when exposed to the surfactant in the extraction liquid. This would weaken the signal from the antigen-antibody reaction. *Acanthamoeba* cysts have been reported to be resistant to some DNA extraction methods used for PCR (34), which would support this theory. Therefore, improvements in the extraction method may increase the sensitivity of assays for *Acanthamoeba* cysts. As the extraction liquid is not able to isolate antigens from solid specimens, the current FICGA kit is available for the analysis of only liquid or semisolid specimens, such as cultures on gel medium, ocular discharge, or corneal scrapings. To further expand the applications of this assay, the extraction method should be improved in further experiments.

The fluorescent intensity of the test line was strongly correlated with the *Acanthamoeba* concentration in the sample. This result suggests that the FICGA kit may have the potential to provide a rough quantitative value of *Acanthamoeba* disease burden, similar to real-time PCR. This information would help clinicians to estimate prognosis and make appropriate treatment decisions (23, 24), although a calibration curve would need to be made. In the current study, the fluorescent intensity of the clinical samples was not quantified because the specialized fluorescent scanner was not available at our facility, and measurements need to be performed within 60 min of the assay. In future studies, it would be of great clinical interest to compare the fluorescent intensity with DNA copy numbers obtained by real-time PCR to determine whether they are correlated in clinical samples. To improve the convenience of our assay, we are now developing a handheld quantitative reader.

In the clinical cases included in this study, the diagnosis of AK was confirmed in all 10 patients by the detection of *Acanthamoeba* DNA with real-time PCR. The FICGA kit detected *Acanthamoeba* antigens in all the samples, including those which tested negative by smear or culture and even in cases with low DNA copy numbers. This suggests that the FICGA can detect *Acanthamoeba* even when there are only a few organisms in the corneal scrapings.

In conclusion, we developed a novel ICGA kit using fluorescent silica nanoparticles for the rapid diagnosis of AK. Our *in vitro* studies suggest that this kit is highly sensitive for the detection of *Acanthamoeba castellanii*, and when the test was applied to clinical specimens, the FICGA results corresponded closely with the results of real-time PCR. Although further evaluation of this technique is needed, the FICGA kit seems to be useful for the diagnosis of AK as it is more rapid and simpler to use than conventional diagnostic procedures, including PCR.

ACKNOWLEDGMENTS

This study was supported in part by a grant for research on emerging and reemerging infectious diseases from the Ministry of Health, Labor and Welfare of Japan (H23-Shinkosaiko-ippan-014).

Hideki Aizawa, Kazutomi Miyoshi, and Michio Ohkubo are employees of Furukawa Electric Co., Ltd. (Tokyo, Japan). The other authors declare no conflicts of interest.